Septiembre 2025

Decoding Cambrian migmatites through their melting and deformation textures: the case of the La Totorilla diatexites, San Carlos Massif, Sierras Pampeanas of Córdoba, Argentina

Alina B. GUERESCHI^{1,2} and Roberto D. MARTINO²

¹Departamento de Geología Básica, Facultad de Ciencias Exactas, Físicas y Naturales, Universidad Nacional de Córdoba (UNC), Córdoba, Argentina.

²Centro de Investigaciones en Ciencias de la Tierra (CICTERRA, CONICET-UNC), Córdoba, Argentina.

Emails: alina.guereschi@unc.edu.ar, roberto.martino@unc.edu.ar

Editor: Ricardo A. Astini Recibido: 03/05/2025

Aceptado: 19/09/2025

ABSTRACT

The La Totorilla anatectic body is located within the San Carlos Migmatitic Massif, part of the Central Granulitic Belt —a regional thermal axis of the Sierras Pampeanas in Córdoba, Argentina. The body has an elliptical shape ($\sim 3 \times 0.5$ km) and consists of foliated, porphyroblastic diatexites rich in potassium feldspar and cordierite, showing clear evidence of melting and deformation. It is enclosed by the Pichanas migmatites, which exhibit a characteristic *schollen* structure. Both lithologies contain *schlieren* and lenticular xenoliths derived from the Tuclame Banded Schists and biotite gneisses. Tourmaline-bearing granitic pegmatite veins cut across these units, locally evolving from boudins into folds. The evolution of the La Totorilla diatexites can be divided into three stages: (1) a prograde phase marked by staurolite—biotite assemblages (~ 600 °C); (2) a metamorphic peak at ~ 788 °C and medium pressure (≤ 6 kbar), characterized by cordierite, K-feldspar, and melt generation through biotite dehydration; and (3) a retrograde stage involving progressive deformation, cooling, and hydration. The penetrative S $_2$ foliation (N 300°) dominates the area and formed under pure-shear flattening. Structurally, the La Totorilla body is boudinaged within the Pichanas migmatites, reflecting a pronounced lithological and rheological contrast. U—Pb zircon rims ages indicate that La Totorilla formed at 532.1 \pm 1.7 Ma during the Pampean orogeny, at middle-crustal levels (≤ 22 km depth), along the southwestern margin of Gondwana. This body constitutes a key example of an anatectic rock recording the interplay of metamorphism, deformation, and partial melting during the early Cambrian evolution of the Sierras Pampeanas.

Keywords: high-grade metamorphism, partial melting, ductile deformation, P-T path, Pampean orogeny.

RESUMEN

Descifrando migmatitas cámbricas a través de sus texturas de fusión y deformación: el caso de las diatexitas La Totorilla, Macizo San Carlos, Sierras Pampeanas de Córdoba, Argentina.

El cuerpo anatéctico La Totorilla se ubica dentro del Macizo Migmático de San Carlos, que es parte de la Faja Granulítica Central, un eje térmico regional en las Sierras Pampeanas de Córdoba, Argentina. Es un cuerpo elipsoidal (~ 3 km × 0,5 km) compuesto por diatexitas porfiroblásticas foliadas, ricas en feldespato potásico y cordierita, con claras evidencias de fusión y deformación. Está rodeado por las migmatitas Pichanas, con una característica estructura tipo *schollen*. Ambas litologías contienen *schlieren* y xenolitos lenticulares derivados de los esquistos bandeados Tuclame y gneises biotíticos. Venas graníticas turmaliníferas pegmatíticas atraviesan las unidades, evolucionando localmente desde boudines hasta pliegues. La evolución de las diatexitas La Totorilla se divide en tres etapas: (1) una etapa prógrada marcada por la asociación de estaurolita y biotita (~ 600 °C); (2) un pico metamórfico a 788 ± 15 °C y presión media (≤ 6 kbar), caracterizado por la generación de cordierita, feldespato potásico y fundido producido mediante la reacción de deshidratación de biotita; y (3) una etapa retrógrada incluyendo deformación progresiva, enfriamiento e hidratación. La foliación

penetrativa S_2 (N 300°) domina el área y se formó por aplastamiento en régimen de cizalla pura. Estructuralmente, el cuerpo de La Totorilla se encuentra boudinado dentro de las migmatitas Pichanas, reflejando un marcado contraste litológico y reológico. La edad U-Pb en circón de 532.1 \pm 1.7 Ma obtenida para las diatexitas La Totorilla indica que se formaron durante la orogenia Pampeana, en niveles de corteza media (\leq 22 km de profundidad), en el margen sudoccidental de Gondwana. Este cuerpo constituye un ejemplo clave de una roca anatéctica que registra la interacción entre metamorfismo, deformación y fusión parcial durante la evolución del Cámbrico temprano en las Sierras Pampeanas.

Palabras clave: metamorfismo de alto grado, fusión parcial, deformación dúctil, trayectoria P-T, orogenia Pampeana.

INTRODUCTION

Anatexis, understood as the differential partial melting of metamorphic rocks in the medium-deep crust, is a fundamental process in the formation of granitic magmas and in the tectonothermal evolution of convergent orogens. This phenomenon develops under specific conditions of temperature, pressure, and fluid presence, and is intimately linked to ductile deformation that facilitates the segregation, migration, and crystallization of melts. A detailed understanding of anatexis is key to interpreting the evolution of the continental crust, as it constitutes an essential mechanism for the recycling and geochemical differentiation of the crust in orogenic environments (cf. Mehnert 1968; Brown and Rushmer 2006; Sawyer 2008a, b; Brown 2013; Pawley et al. 2015).

The Sierras Pampeanas of Córdoba, located in northcentral Argentina, represent an exceptional area for studying anatectic processes owing to their igneous-metamorphic basement, which is characterized by extensive migmatitic areas (Fig. 1). Within this region, the Central Granulitic Belt stands out as a regional thermal axis that recorded high-temperature metamorphism and penetrative ductile deformation (Guereschi and Martino, 2014, and references therein). In its northwestern sector, the San Carlos Migmatitic Massif (Gordillo 1979; Fig. 1) is dominated by garnet- and cordierite-bearing diatexites, which Gordillo (1984) referred to as "tonalitic migmatites" because of their low or absent potassium feldspar content. In contrast to these tonalitic varieties, small anatectic bodies of granitic composition -rich in potassium feldspar and aluminum-bearing minerals, with a coarse-grained, plutonic appearance— occur within the San Carlos Massif. These bodies, typically a few kilometers across, mark local domains of partial melting of more pelitic protoliths within the regional migmatitic complex. Some of the most important anatectic bodies are El Pilón (Rapela et al. 2002), Juan XXIII (Martino et al. 2004, 2005), La Totorilla (this work), Bella Vista, and Piedra Blanca (Guereschi and

Martino 2014 and references therein). Despite advances in the characterization of the migmatites of the San Carlos Massif, significant uncertainties persist regarding the physical and chemical conditions controlling anatexis, as well as the interaction between metamorphic and deformational processes during the formation and evolution of the small anatectic bodies. In particular, the relationship between partial melting and ductile deformation, the growth dynamics of potassium feldspar porphyroblasts, and the precise chronology of metamorphic and deformational events require detailed and integrated analysis. The La Totorilla anatectic body, located 11 km west of the town of La Higuera (Minas Department, Córdoba Province), provides an exceptional opportunity to address these questions despite its small dimensions (Fig. 1). The study of this body enables the integration of petrographic, mineral-chemical, geochronological, and structural data to reconstruct the evolution of anatexis within a complex orogenic context. The La Totorilla exposure is currently exploited in an open-pit quarry for ornamental stone extraction, which provides excellent outcrop conditions for detailed investigation —an advantage over other, vegetation-covered sectors of the massif. In the Villa Dolores geological map, Bonalumi et al. (1999) briefly described the La Totorilla anatectic body and classified it as an anatectic granite comparable to the nearby El Pilón occurrence (Rapela et al. 2002).

The working hypothesis proposed here is that the La Totorilla anatectic body does not represent an igneous granitoid but rather a metamorphic rock of anatectic origin, produced by *in situ* partial melting of pelitic protoliths during the early Cambrian. This process would have occurred under ductile deformation conditions associated with the Pampean orogeny along the southwestern margin of Gondwana. This interpretation challenges earlier classifications that regarded the body as an intrusive granite (Bonalumi et al. 1999) and instead proposes an integrated model in which metamorphism, anatexis, and deformation were coeval processes in the evolution of the middle to lower crust during the Pampean orogeny.

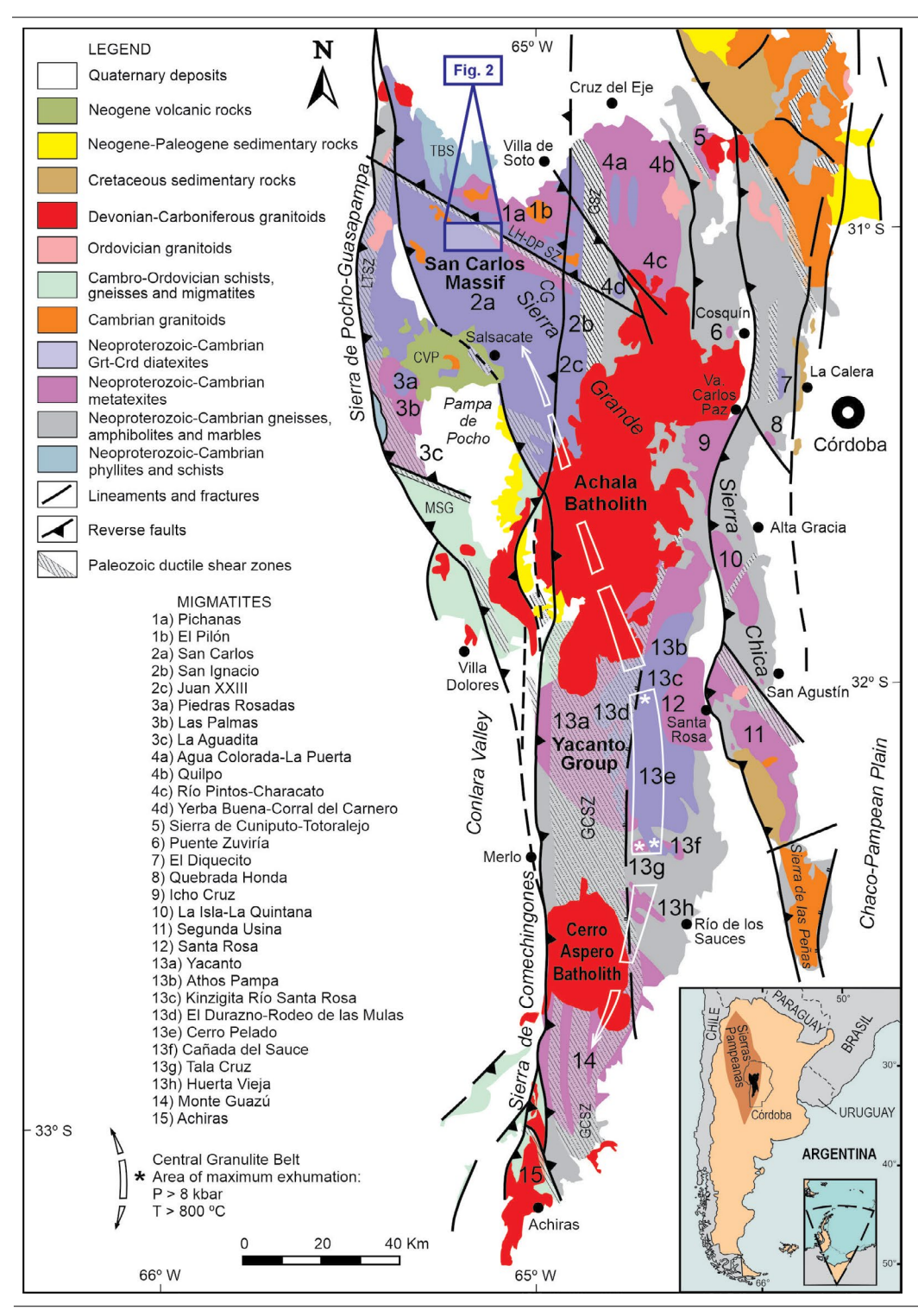


Figure 1. Geological map of the Sierras Pampeanas of Córdoba showing the location of the main migmatite outcrops (modified from Guereschi and Martino 2014). The box indicates the location of the study area and the map shown in Figure 2. CG: Cumbre de Gaspar, CVP: Pocho Volcanic Complex, GCSZ: Guacha Corral shear zone, GSZ: Guamanes shear zone, LH-DP SZ: La Higuera-Dos Pozos shear zone, LTSZ: Los Túneles shear zone, MSG: Mogigasta Schists and Gneisses, TBS: Tuclame Banded Schists.

The objectives of this study are to: (1) characterize the field relationships, petrography, mineral chemistry, peak metamorphic age, and structural features of the La Totorilla anatectic body and its host rocks; (2) estimate the physical conditions under which it formed; (3) reconstruct its tectonothermal evolution; and (4) establish regional correlations within the San Carlos Migmatitic Massif and the broader geological framework of the Sierras de Córdoba,

thereby providing new insights into partial melting and deformation processes in the middle to lower crust of the Sierras Pampeanas.

GEOLOGICAL FRAMEWORK

The Sierras de Córdoba are the easternmost range of

the Argentine geological province known as the Sierras Pampeanas (Fig. 1). They extend for approximately 500 km in length and 150 km in width, between 29° 00'-33° 30' south latitude and 64° 00'-65° 30' west longitude. These ranges are composed of a series of mountain chains formed by a polydeformed metamorphic basement of late Proterozoic to early Paleozoic age (Gordillo and Lencinas 1979, Guereschi and Martino 2014, Martino and Guereschi 2014, and references therein). During the middle Paleozoic (Ordovician-Silurian) and late Paleozoic (Devonian-Carboniferous), this basement was imbricated by contractional ductile shear zones (Martino 2003) and intruded by granitoids such as the Achala Batholith (Lira and Sfragulla 2014). On the western margin, at the foot of the Sierra de Pocho, small outcrops of continental sedimentary rocks of Carboniferous-Permian age are found. To the east, in the Sierra Chica, there are large exposures of continental red beds, together with Cretaceous basaltic dikes and flows (Astini and Oviedo 2014, Lagorio et al. 2014). The mountain ranges are oriented north-south and are bounded by west-vergent Tertiary reverse faults, being separated by intermontane basins filled with Mesozoic and Cenozoic sediments. The entire system rises from the Quaternary Chaco-Pampean plain. In the central-western sector, a prominent assemblage of Neogene trachyandesitic volcanic rocks and associated pyroclastic deposits (Arnosio et al. 2014) overlies a landscape of crustal blocks tilted eastward by the aforementioned faults.

The metamorphic basement is predominantly composed of migmatites -both diatexites and metatexites- and biotite tonalitic gneisses, which commonly contain garnet and, less frequently, sillimanite. Garnet-cordierite diatexites represent the main lithologies of the Central Granulitic Belt, a regional thermal axis extending over more than 3,000 km² and trending NNW. This belt is bordered by metatexites and gneisses and is locally disrupted by the Achala Batholith (Fig. 1). In the southeastern sector of the Central Granulitic Belt lies the Yacanto Group of the Sierra de Comechingones Complex (Martino et al. 1995, Bonalumi et al. 1999), which partially overlaps with the Calamuchita Complex (Otamendi et al. 2004). In this area, the deepest, highest-temperature, and oldest rocks of the Neoproterozoic-Cambrian crust of the Sierras de Córdoba are exposed (Siegesmund et al. 2010, Guereschi and Martino 2014, Barzola et al. 2021). The main structure in migmatites and gneisses is a stratiform, highly penetrative, regionally distributed metamorphic foliation called S₂. A relict S1 foliation, formed during the M1–D1 metamorphic event, is locally preserved in intrafolial folds and as inclusions within garnet porphyroblasts. The S₂ foliation developed during the main metamorphic event (M2-D2) of the Pampean

orogeny and was subsequently overprinted by intense non-coaxial ductile deformation (D3) under high-temperature conditions, resulting in shear-related folding (Martino and Guereschi 2014).

In the northwestern sector of the Central Granulite Belt lies the San Carlos Migmatitic Massif (Gordillo 1984), which extends over an area exceeding 1,500 km² and is bounded to the east by the Cumbre de Gaspar and to the west by the Sierra de Pocho-Guasapampa (Fig. 1). The predominant lithology consists of garnet-cordierite 'tonalitic' diatexites, whereas metatexites are less abundant. Paleosomatic remains of banded schists, biotite gneisses, calc-silicate granulites, marbles, amphibolites, quartzites, and mafic and ultramafic rocks are also present (Guereschi and Martino 2014). Within the San Carlos Massif, several anatectic bodies of granitic composition and plutonic appearance occur as lenticular or irregular outcrops smaller than 100 km², including Juan XXIII (Martino et al. 2004, 2005), El Pilón (Rapela et al. 2002), La Totorilla (Palavecino 2020, Guereschi et al. 2024), Piedra Blanca, and Bella Vista, among others (Guereschi and Martino 2014). Geochronological data from the El Pilón granitoid (523 ± 4 Ma, Rapela et al. 1998; 526.9 ± 4 Ma, Stuart-Smith et al. 1999) indicate an early Cambrian age, which has been extended by correlation to the other similar anatectic bodies (Bonalumi et al. 1999).

In the northern sector of the San Carlos Migmatitic Massif, there is an extensive body of migmatites displaying a *schollen* structure —characterized by blocks of residual paleosome dispersed within anatectic leucosomes (Mehnert 1968)—originally described by Sureda (1978) and later included within the Pichanas Migmatites (Guereschi and Martino 2014). Over these rocks, the La Higuera—Dos Pozos ductile shear zone (LH–DP SZ in Fig. 1) developed, trending northwest and showing overall reverse kinematics with a subordinate sinistral strike-slip component (Martino 2003).

The Tuclame Banded Schists (Martino et al., 2009) form a belt several tens of kilometers wide in the northwestern sector of the Sierras de Córdoba (TBS in Fig. 1). These rocks are characterized by a particular internal structure given by a tectonic banding that is discordant with the dominant S_2 foliation of the regional migmatites. Other outcrops of similar size are found in the Sierra de Altautina (Altautina schists) and in the Sierra de Pocho (forming part of the Mogigasta Schists and Gneisses, MSG in Fig. 1). Smaller outcrops, in the form of inclusions and xenoliths ranging from decametric to centimetric size, are widely distributed in the Pichanas migmatites and in the aforementioned anatectic granitoid bodies such as El Pilón, Juan XXIII, La Totorilla, and others. Banded schists with characteristics similar to those of Tuclame

have also been recognized in the Sierra de San Luis (as part of the Conlara Metamorphic Complex, Manchento et al. 2024 and references therein), and are widely distributed in other areas of the Sierras Pampeanas, mainly in its eastern sector, and in the Puna (Martino et al. 2009 and references therein).

METHODOLOGY

Seventeen rock samples were collected from the La Totorilla anatectic body and surrounding rocks, both oriented (for structural analysis) and unoriented. Fifteen thin sections were prepared at the LabGeo (Facultad de Ciencias Exactas, Físicas y Naturales, CICTERRA–UNC, Córdoba, Argentina) from these samples for microscopic analysis. Macroscopic description involved determining the mineralogy, structure, and degree of alteration of the different lithologies. Microscopic description focused on detailed mineral identification, textural relationships, and microstructures within the rocks. This approach allowed us to determine the mineral parageneses and the metamorphic reactions responsible for their formation.

Arepresentative sample (#1017) was selected to determine the chemical composition of the main mineral phases of the La Totorilla anatectic body. Analyses were performed using a Jeol JXA 8230 electron microprobe at the Laboratorio de Microscopía Electrónica y Análisis por Rayos X (LAMARX, CONICET–UNC) in Córdoba, Argentina. Standard operating conditions were used: 15 kV accelerating voltage, 20 nA beam current (10 nA for feldspars), and a 3–5 µm beam diameter, with both natural minerals and synthetic compounds as standards.

Sample #1017 was also analyzed to determine its age using the U-Pb method on zircons. The analysis was conducted at the LaTe Andes S.A. Laboratory in Salta, Argentina. Zircons were hand-picked, mounted in resin, and polished. Grains without inclusions or fractures were selected. A combination of LA-ICP-MS (laser ablation inductively coupled plasma mass spectrometry) was used: a 193 nm RESOlution laser ablation system (Australian Scientific Instruments) and an Agilent 8900 triple quadrupole ICP-MS. The spot diameter was 24 um, and generally one spot per zircon was measured. U-Pb ages were calculated from isotopic ratios using zircons 91500 (Wiedenbeck et al. 2004) and Plešovice (Sláma et al. 2008) as reference materials. Common Pb corrections were applied according to the two stage isotope evolution model of Stacey and Kramers (1975). Calculations and plots were performed using Isoplot 4.15 (Ludwig 2008) and IsoplotR (Vermeesch 2018).

FIELD RELATIONSHIPS

The La Totorilla anatectic body has an elliptical shape in plan view, with a major axis of approximately 3 km oriented northwest and a minor axis of 0.5 km (Fig. 2a). The body is topographically elevated and outcrops as rounded blocks or boulders. The southwestern contact is sharp and well-defined, oriented N 315° and dipping 75–90° to the northeast. In contrast, the northeastern boundary is diffuse and difficult to discern due to dense vegetation.

The La Totorilla body is composed of foliated porphyroblastic diatexites, which outcrop as large rounded or elongated boulders trending northwest, forming the typical "whale-back" shapes characteristic of migmatitic areas (Fig. 3a). Within the body, three mutually orthogonal joint sets are consistently developed. The rocks stand out by their pinkish-gray color (Fig. 3b), due to the dominant presence of large potassium feldspar crystals (up to 5 cm long), which sometimes form aggregates resembling leucosomes up to 2 cm thick. These crystals, together with biotite and quartz, define a coarse $\rm S_2$ foliation trending northwest (N 300°) and steeply dipping (80–90°) to the southwest and northeast, parallel to the contacts of the body (Fig. 2a, b).

Within the La Totorilla body, lenticular xenoliths derived from the Tuclame Banded Schists and biotite gneisses, ranging from meter to decameter scale, are arranged following the general $\rm S_2$ foliation (Fig. 3c, d). In some cases, these xenoliths are fragmented and form biotite *schlieren*. At the contact between the diatexites and xenoliths, conspicuous festooned or mullion structures are observed, with cusps pointing toward the diatexites (Fig. 3c, d). Rare xenoliths of stromatic metatexites, with coarse-grained, pink, and quartz–feldspar leucosomatic layers transitioning into the diatexites, are also present (Fig. 3e).

To the northwest of the La Totorilla body (Fig. 2a), a small elongated body of biotite monzogranite outcrops, measuring approximately 150 m long and 40 m wide, white in color, medium grain in size, and exhibiting a coarse S_2 foliation. This body also outcrops as elongated boulders trending northwest.

The rocks surrounding and enclosing both bodies are the Pichanas migmatites (Guereschi and Martino 2014). This lithological unit forms a broad belt oriented N 320°, approximately 18 km long and 8 km wide, extending beyond the area shown in Figure 2a. It consists of granitoid composition rocks ranging from whitish-gray to grayish-white, medium-grained, with abundant elliptical xenoliths derived from the Tuclame Banded Schists and biotite gneisses (Fig. 3g). These features give rise to the general raft- or *schollen*-

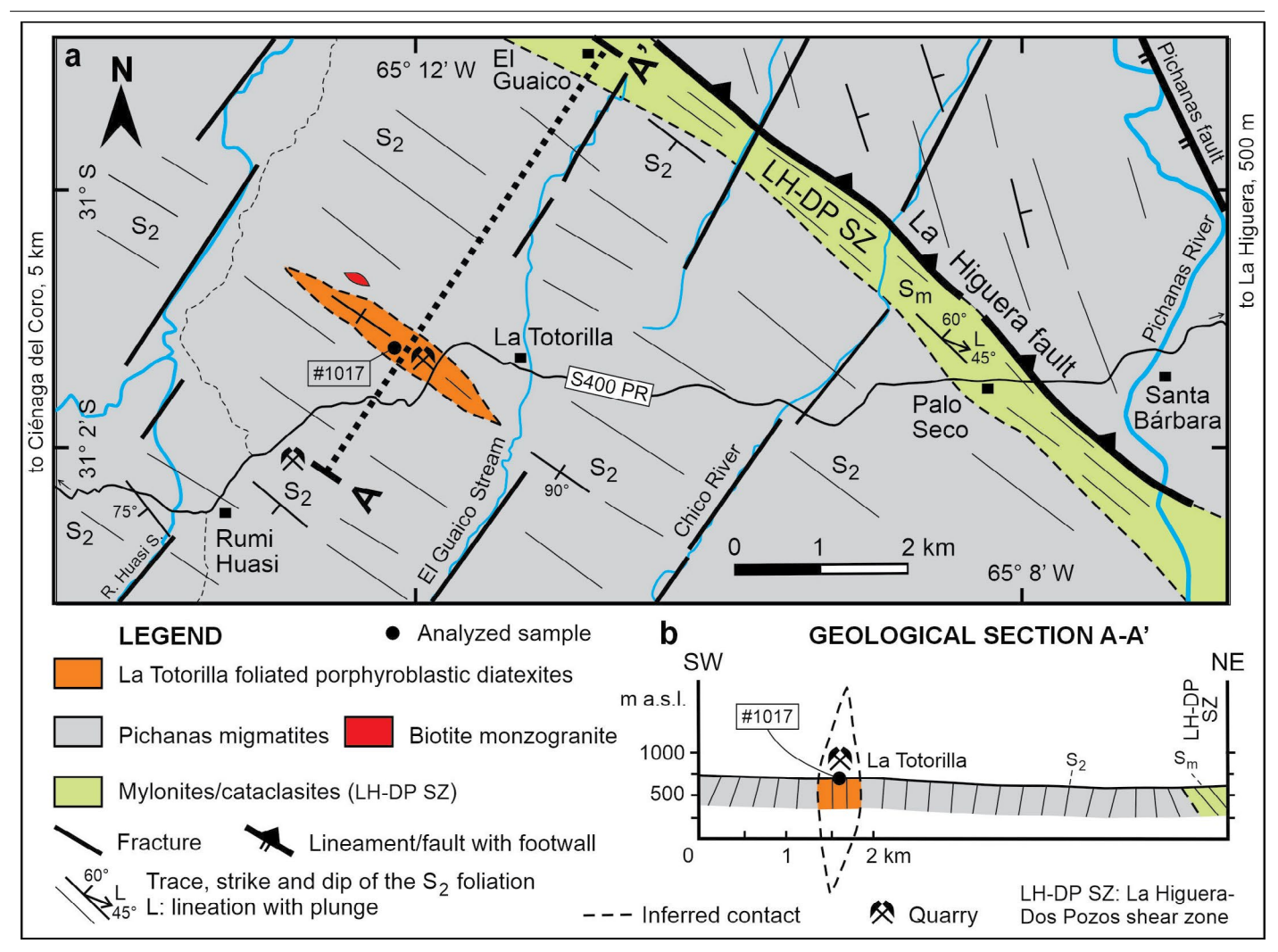


Figure 2. (a) Geological map and (b) geological section A-A' showing the lenticular shape of the La Totorilla anatectic body.

type migmatitic structure (Mehnert 1968, Sawyer 2008a, b) noted by Sureda (1978) around the El Guaico mining district. The xenoliths have their long axes parallel to a penetrative $\rm S_2$ foliation affecting all Pichanas migmatites, oriented N 320° and dipping 70° to the southwest. In many cases, the xenoliths are fragmented and form biotite schlieren parallel to the $\rm S_2$ foliation. In some sectors, such as the southwestern contact of the La Totorilla body, the Pichanas migmatites exhibit a marked gneissic fabric. To the southwest of La Totorilla, near the Rumi Huasi locality (Fig. 2a), migmatites with net-like to schollen structures (Mehnert 1968, Sawyer 2008a, b) outcrop, containing abundant cordierite nodules and rare garnet relics within plagioclase (Lescano 2019).

Additionally, tourmaline-bearing granitic veins (Fig. 3f) with very coarse (pegmatoid) texture, decimetric and irregular thicknesses, cut across both the La Totorilla foliated porphyroblastic diatexites and the Pichanas migmatites. These veins show varying degrees of deformation (see Structure Section) and are oriented either transversely or longitudinally

to the dominant S₂ foliation.

It should be noted that the lithological assemblage of the studied area has an overall granitoid composition, dominated by potassium feldspar, plagioclase, quartz, and biotite. These rocks exhibit pink, white, and gray colors corresponding to the La Totorilla foliated porphyroblastic diatexites, the biotite monzogranite, and the Pichanas migmatites, respectively. Furthermore, all these rocks are intensely deformed, developing the same coarse S_2 foliation trending northwest and outcropping as elongated boulders. These compositional and outcrop features shared by all rocks, combined with the abundant vegetation, complicates the field relationships (identification of contacts and rock-types).

PETROGRAPHY

The following section provides a detailed description of the rocks from the La Totorilla anatectic body, classified as foliated

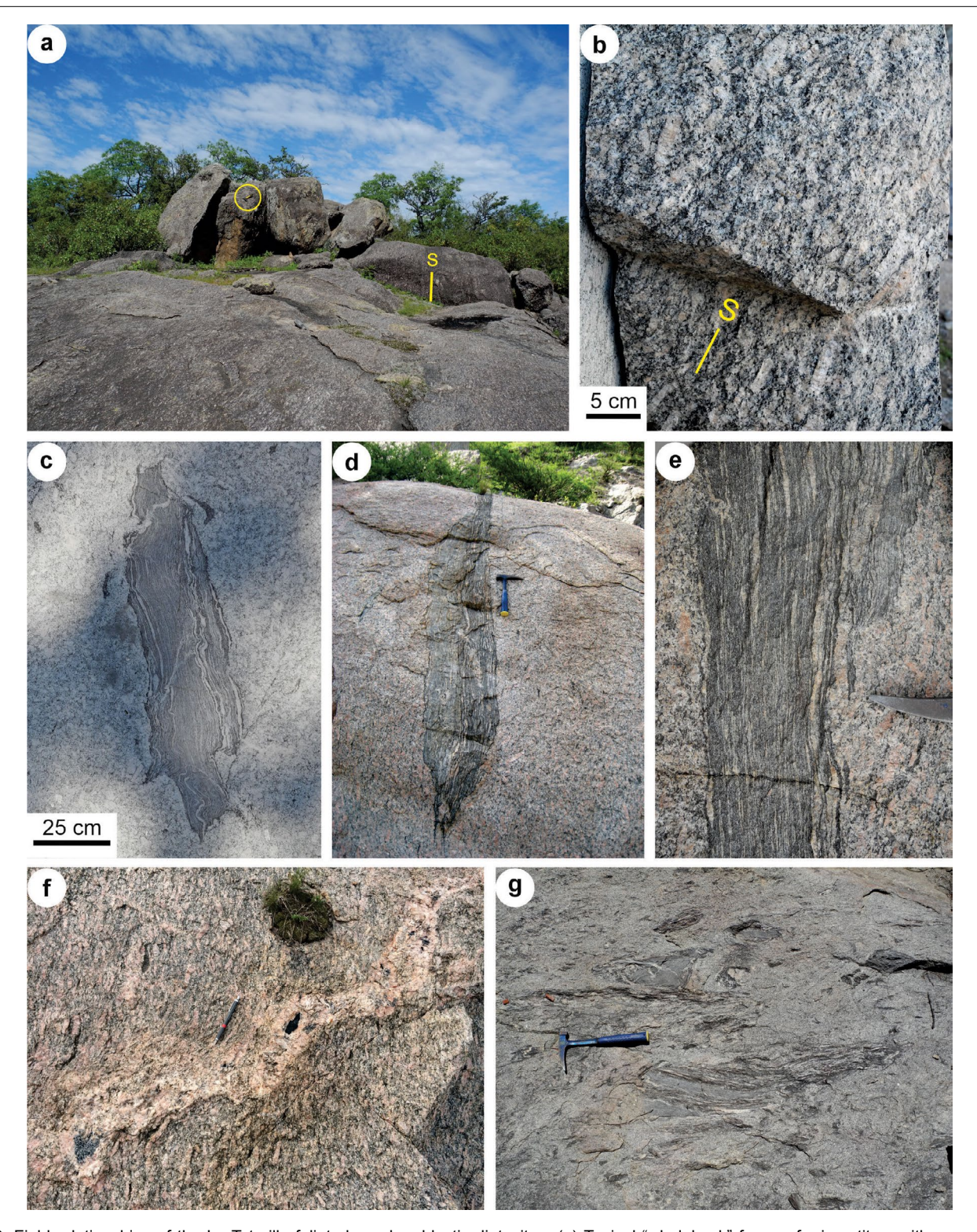


Figure 3. Field relationships of the La Totorilla foliated porphyroblastic diatexites. (a) Typical "whaleback" forms of migmatites, with coarse, nearly vertical foliation (S_2). Note the abundant vegetation. Scale hammer: 30 cm long (circle). (b) Vertical section facing N 300°, in a quarry face, showing the pinkish-gray color of fresh rock and the foliated S_2 fabric, marked by potassium feldspar porphyroblasts (< 5 cm long) bordered by biotite-rich bands. (c, d, e) Lenticular xenoliths, elongated along S_2 , composed of Tuclame Banded Schists (c) and stromatic metatexites (d, e). Biotite *schlieren* and mullions occur at the xenolith contacts, with cusps pointing toward the diatexites (arrows). Hammer length: 30 cm. (e) Detail of stromatic metatexite xenoliths, with coarse-grained, pink, quartz–feldspar leucosomes transitioning into diatexites (pointed out by the hammer's pick end). (f) Tourmaline granitic veins (pegmatoids), decimeter in thick, irregular in shape, and both transverse and longitudinal to the dominant S_2 foliation —gently folded— of the La Totorilla diatexites. Scale pencil: 15 cm long. (g) Plan view of an outcrop of Pichanas migmatites, with *schollen* structure and gray color. Numerous ellipsoidal metamorphic xenoliths and biotite *schlieren* are visible, all parallel to the penetrative S_2 foliation, oriented N 320° (marked by scale hammer: 30 cm).

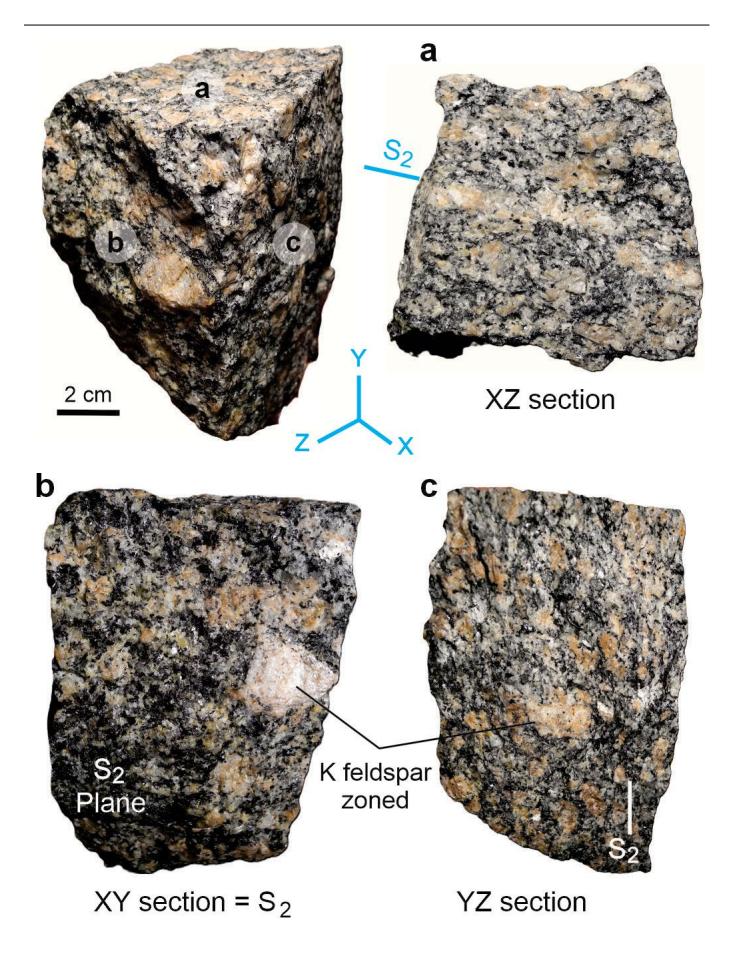


Figure 4. Photographs of a three-dimensional block of the La Totorilla foliated porphyroblastic diatexites, showing the planar S_2 fabric of the rock in three perpendicular sections, related to the finite strain axes X, Y, Z. In sections perpendicular to S_2 (a, c), potassium feldspar porphyroblasts have tabular shapes, irregular edges, and two-individual twins. In sections parallel to S_2 (b), the porphyroblasts are flattened or oblate with irregular edges.

porphyroblastic diatexites. In addition, brief descriptions of the white granitoid body, classified as biotite monzogranite, as well as the Pichanas migmatites surrounding both bodies (Fig. 2a) are included.

La Totorilla foliated porphyroblastic diatexites

In hand samples, these rocks are pinkish gray in color and exhibit a general planar fabric S₂. They are characterized by the abundance of large potassium feldspar crystals (porphyroblasts) up to 5 cm in size, pink in color and oriented parallel to S_2 . In sections cut perpendicular to S_2 , the porphyroblasts have tabular shapes, irregular edges, and simple two-individual twins. In sections parallel to S₂, the porphyroblasts appear flattened or oblate with irregular edges (Fig. 4). Some porphyroblasts show zoning marked by trains of inclusions, mainly biotite. Locally, aggregates of potassium feldspar with quartz or pure potassium feldspar occur as veins up to 2 cm wide and 10 cm long (leucosomes). Locally, these leucosomes are bordered by thin biotite-rich bands (melanosomes) that impart a stromatic structure to the rock. Around the porphyroblasts and leucosomes, a coarse-grained (up to 4 mm) matrix is composed of quartz, potassium feldspar, plagioclase, biotite, sillimanite, and cordierite. Thin biotite bands (< 0.5 cm wide) outline the feldspars. These elements define the S₂ mesoscopic foliation of the rock (Fig. 3b), with a strike of N 300° and a steep dip toward the southwest (locally up to 90°).

The general texture is porphyroblastic, with well-developed potassium feldspar porphyroblasts in a coarse-grained granolepidoblastic matrix (up to 4 mm; Fig. 5a, b). All matrix blasts are elongated and anastomosed around

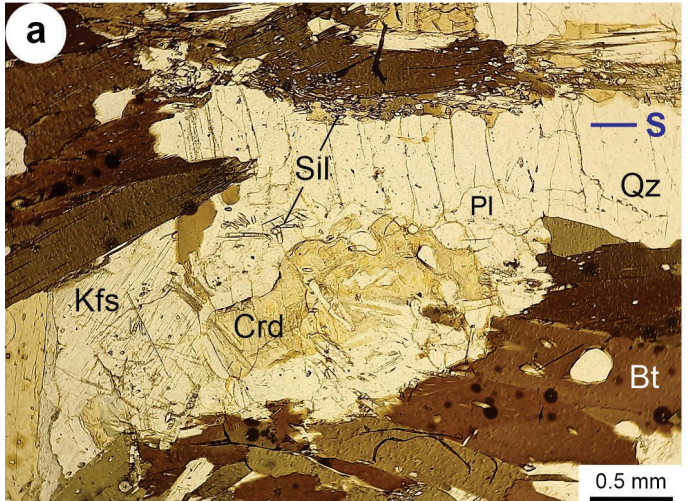




Figure 5. Photomicrographs of the La Totorilla foliated porphyroblastic diatexites, under plane-polarized (a) and cross-polarized (b) light. Matrix with coarse-grained granolepidoblastic texture composed of quartz, biotite, plagioclase, sillimanite, potassium feldspar, and cordierite (partially pinitized), resulting from the main anatectic reaction. Elongation of minerals along the S_2 foliation, formation of fibrolite associated with shear deformation along the basal plane of biotite and the presence of secondary muscovite are observed.

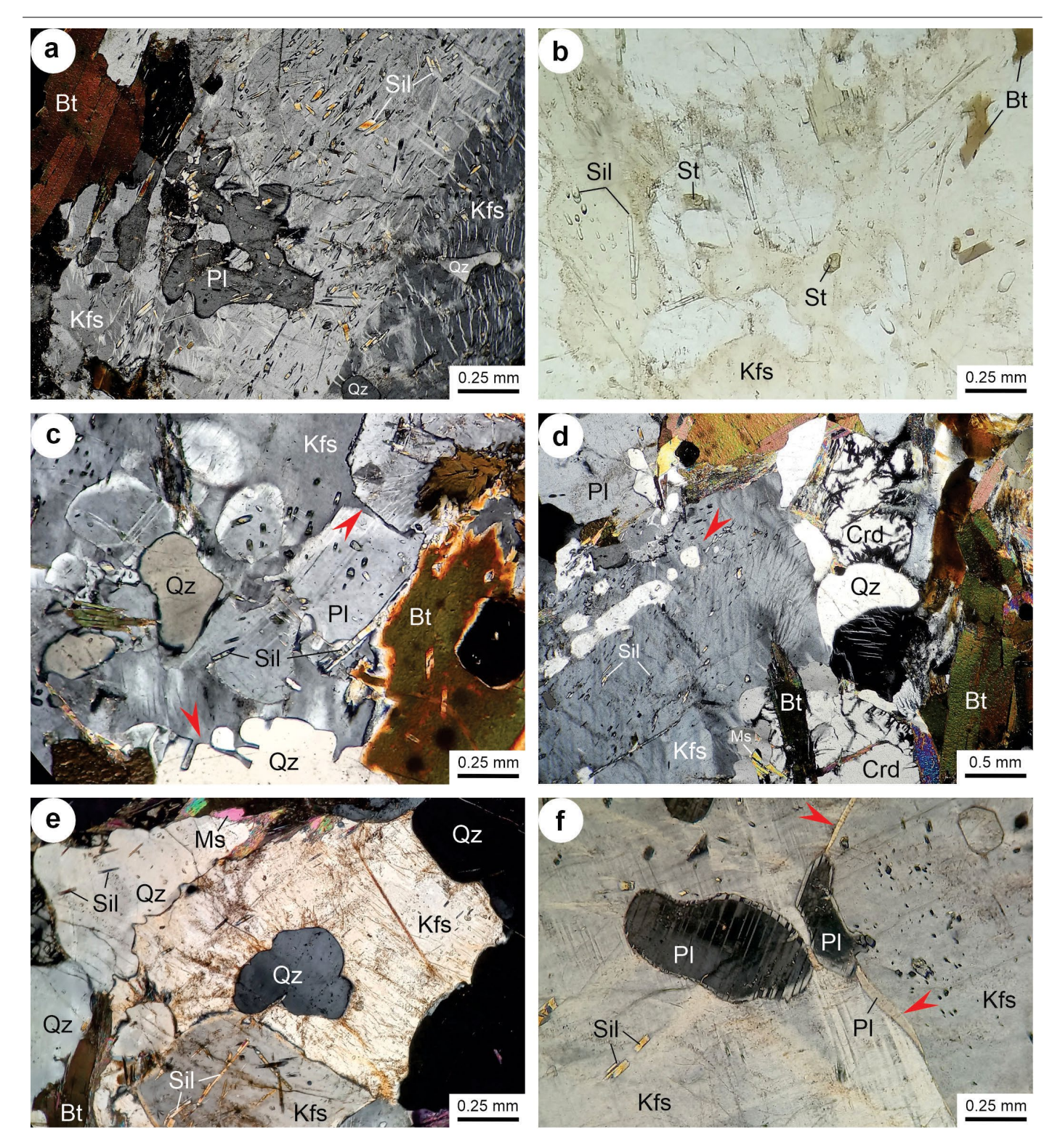


Figure 6. Photomicrographs of the La Totorilla foliated porphyroblastic diatexites, under cross-polarized (a, c, d, e, f) and plane-polarized (b) light. (a) Perthitic potassium feldspar porphyroblast with two-individual twinning, containing inclusions of biotite, sillimanite, quartz, and plagioclase (reactant minerals) with lobate contacts. (b) Relict staurolite and microboudinaged sillimanite inclusions within potassium feldspar. (c) Detail of reaction texture from melting of biotite, sillimanite, quartz, and plagioclase that generated potassium feldspar. In contact with plagioclase and quartz, low dihedral angle lamellae (arrows) and festooned edges with cusps toward both minerals are formed. (d) Similar to (c), showing concomitant generation of cordierite and string of beads texture of quartz at the edge of perthitic potassium feldspar (arrow). (e) Melting texture marked by festooned contacts between potassium feldspar and quartz, with cusps pointing toward the latter. (f) Detail of potassium feldspar with inclusions of microboudinaged sillimanite and plagioclase with reaction rims. Tabular to sigmoidal plagioclase lamellae with low dihedral angles are observed in contact with potassium feldspar (arrows).

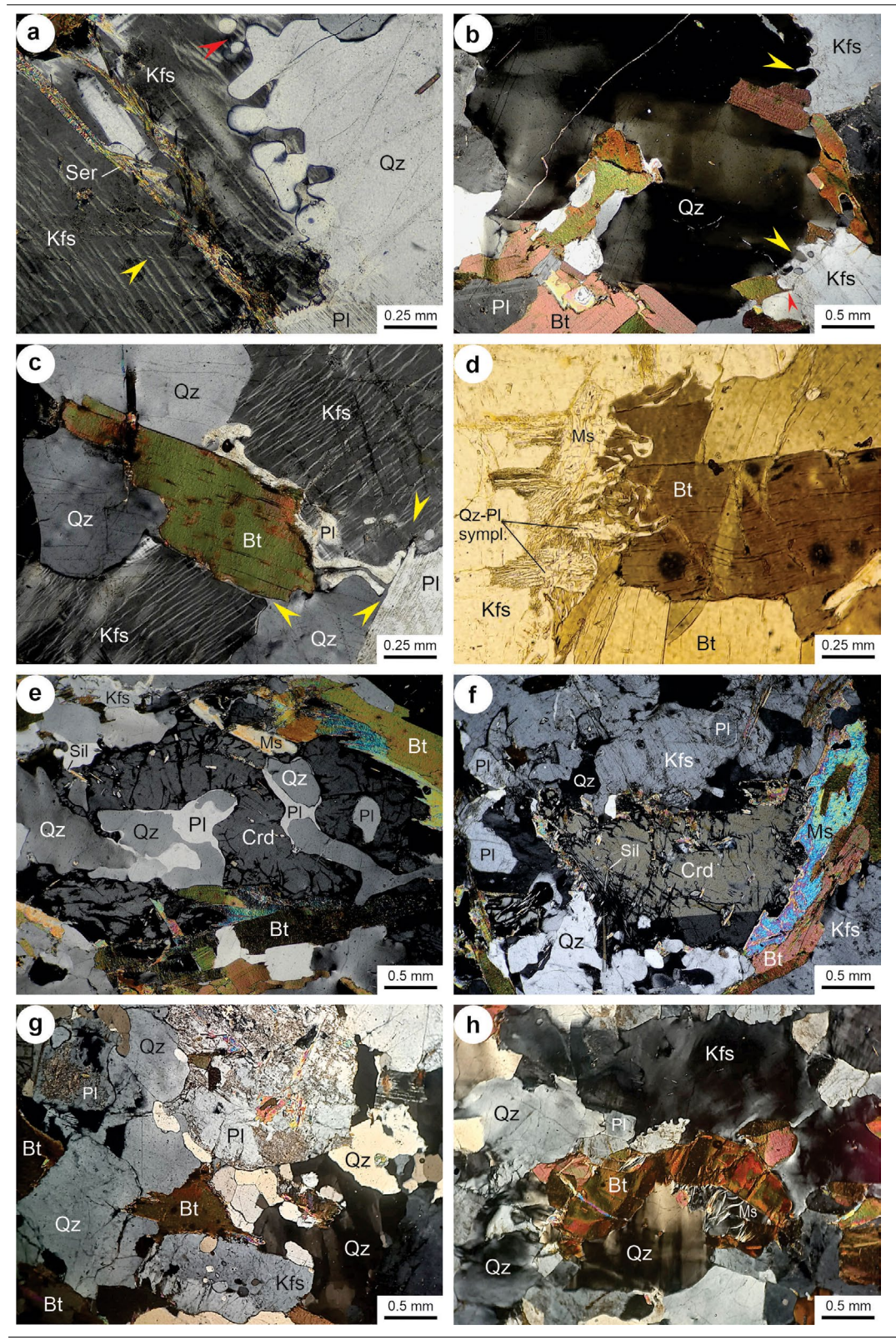


Figure 7. Photomicrographs of the La Totorilla foliated porphyroblastic diatexites, under cross-polarized light. (a) Melting texture marked by lobate contacts between quartz and potassium feldspar, showing an incipient string of beads texture (upper arrow). The potassium feldspar shows deformation with undulatory extinction and blurred perthites displaced by microkink bands (lower arrow). (b) Deformed quartz with chessboard undulatory extinction texture. Lamellae with low dihedral angles and lobate contacts with potassium feldspar (upper arrow), incipient string of beads texture (central arrow), and pointed contacts with plagioclase and biotite (lower arrow). Irregular fractures filled with sericite. (c) Detail of melting reaction texture of biotite that generated potassium feldspar, vermicular plagioclase, and quartz. Characteristic granitic melt contacts such as low dihedral angles and string of beads texture are visible (arrows). (d) Quartz plagioclase symplectites, partially muscovitized, at biotite edges in reactive contact with potassium feldspar. Kink bands deformation is observed in biotite. (e) Intergrowth of cordierite with quartz-plagioclase-potassium feldspar, products of the melting reaction. Notable are the particular contact relationships among these minerals, especially low-dihedral angles in plagioclase. (f) Twinned cordierite with sillimanite inclusions, in contact with potassium feldspar, quartz, and plagioclase. Present muscovite is secondary. (g) and (h) Textural and mineralogical features of the biotite monzogranite and the Pichanas migmatites respectively (see details in the

the potassium feldspar porphyroblasts and veins, defining the foliation. In addition to shape orientation, a coarse crystallographic orientation is observed in the potassium feldspar porphyroblasts.

Potassium feldspar occurs in two textural types. (1) Xenoblasts in the matrix with rounded shapes, medium

grain size (< 3 mm), undulatory extinction, and inclusions of plagioclase and quartz. (2) Tabular porphyroblasts up to 5 cm, with irregular to lobate edges, flame perthitic textures, well-developed two-individual twins, and diffuse grid twins (Fig. 6a). They are poikilitic, containing numerous inclusions of quartz, biotite, sillimanite, plagioclase (with a thin reaction rim

at the contact with potassium feldspar, Fig. 6c, f), cordierite, apatite, and staurolite (Fig. 6b). Some porphyroblasts show zoning marked by the orientation of rounded biotite sheets resembling droplets. At their edges, rounded quartz and plagioclase inclusions (blebs) form a string of beads texture (Figs. 6d and 7a). In contact with plagioclase or quartz, they form pointed lamellae with low dihedral angles and festooned edges with cusps toward both minerals (Fig. 6c), while in contact with biotite, symplectic textures are formed (Fig. 7d). Undulatory extinction is recognized, while twins and perthites are blurred and displaced by microkink bands (Fig. 7a, c). The degree of alteration is generally low, mainly to kaolinite.

Plagioclase also occurs in two textural types. (1) Subidioblastic tabular grains of fine size (< 0.5 mm), with straight to rounded outlines, a thin rim of different composition (Fig. 6c, f), undulatory extinction, and both simple and polysynthetic twins that are blurred. These grains are often included within potassium feldspar porphyroblasts. (2) Tabular xenoblasts of medium size (1 to 3 mm), showing slight zoning (rim of different composition at the contact with potassium feldspar) and twins (simple and polysynthetic, Fig. 6c). They contain inclusions of biotite, quartz, potassium feldspar, sillimanite, cordierite, and apatite. In contact with quartz, they have festooned edges with cusps pointing toward the quartz, while in contact with other plagioclase crystals, the edges are straight. At their edges, rounded inclusions (blebs) of quartz and biotite are identified, sometimes forming a string of beads texture. In contact with potassium feldspar, and locally, myrmekitic textures and tabular to sigmoidal lamellae with low dihedral angles are observed (Fig. 7c, e). They exhibit undulatory extinction, deformation of twinning (wedging, bending, and blurring), kink bands (Fig. 7d), and fractures perpendicular to the twins filled with muscovite and green biotite. The degree of alteration is low, mainly to sericite.

Quartz appears as xenoblasts of medium to coarse size (< 4 mm), elongated following the orientation of foliation, with scarce biotite inclusions (Fig. 5a, b). In contact with potassium feldspar and plagioclase, it has festooned edges with cusps pointing toward itself and low dihedral angles (Figs. 6c, e and 7a, b). It also forms a vermiform texture that transitions into a string of beads texture (Figs. 6d and 7a). It exhibits deformation bands and chessboard extinction (Fig. 7b), lobate edges, and finer polygonal grains with triple junctions surrounding a larger deformed grain (mantle and core texture). Fractures filled with oxides and sericite are present (Fig. 7b).

Biotite shows pleochroism ranging from light to dark brown, and occurs in two textural types. (1) Fine subidioblastic to xenoblastic sheets (< 0.5 mm), tabular to rounded or droplet in shape, occurring as inclusions within potassium feldspar,

plagioclase, and quartz. (2) Medium to coarse subidioblastic sheets (< 4 mm), containing inclusions of sillimanite, zircon/monazite, and apatite (Fig. 5a, b). It presents quartz symplectites toward potassium feldspar and cordierite, occurring as inclusions within them (Fig. 7d). Intergrown with sillimanite, it forms bands preferentially oriented parallel to foliation (Fig. 5a, b) and bordering potassium feldspar porphyroblasts. It is bent, shows undulatory extinction, ragged edges, and kink bands (Fig. 7d); it also occurs as sigmoidal lenses. The degree of alteration is low, mainly to green biotite, with muscovite replacement at edges and opaque mineral exsolutions.

Cordierite forms coarse xenoblasts (up to 4 mm), elongated with preferred orientation according to the foliation, lobate edges, and undulatory extinction. It is occasionally twinned (Fig. 7f). It contains inclusions of sillimanite, plagioclase, quartz, biotite, apatite, and zircon/monazite. Smaller blasts are included within quartz, plagioclase, and potassium feldspar. The degree of alteration is moderate to high, with pinite at edges and fractures, and green biotite and muscovite also present at edges (Figs. 5a, b; 6d and 7e, f).

Sillimanite is prismatic to acicular (Fig. 5a, b), fine grain size (< 0.5 mm), and partially altered to sericite. It occurs as inclusions within potassium feldspar, plagioclase, and cordierite (Figs. 6a, b, c and 7f); it is also associated with biotite marking the foliation. The prismatic variety is microboudinaged within micas and feldspars (Fig. 6b). The fibrolitic variety surrounds the prisms or occurs as inclusions.

Accessory minerals commonly found are apatite and zircon/monazite. Very fine grains of staurolite included within potassium feldspar are also identified (Fig. 6b).

Alteration minerals include green biotite, pinite, muscovite, sericite, and scarce opaque minerals along biotite cleavage planes and edges. In particular, muscovite forms subidioblastic to xenoblastic sheets, medium-sized (< 2 mm), with lobate and bent edges (Fig. 5a, b). It exhibits symplectic textures in contact with quartz and potassium feldspar.

Biotite monzogranite

In hand sample, the rock is white to whitish gray in color and medium to coarse grain in size, containing large tabular crystals (< 3 cm) of muscovite and biotite. Thin veins of black tourmaline (schorl) and irregular aggregates of tourmaline and muscovite forming centimeter-sized nodules are observed. A very coarse (S_2) foliation is present, although poorly defined and difficult to recognize, marked by the preferred orientation of biotite.

The overall texture is porphyritic, with phenocrysts of potassium feldspar in a coarse-grained (< 4 mm) xenomorphic

matrix composed of quartz, potassium feldspar, plagioclase, biotite, and secondary muscovite (Fig. 7g).

Potassium feldspar forms coarse-grained, xenomorphic crystals with lobate edges, flame perthitic and patchy textures, undulatory extinction, and diffuse and bent grid twinning. Quartz occurs as medium- to coarse-grained (< 4 mm) xenomorphic crystals with inclusions of rutile, biotite, and zircon/monazite. Undulatory extinction, deformation bands, chessboard extinction, and finer polygonal grains with triple junctions are recognized. Plagioclase appears as subidiomorphic to xenomorphic tabular crystals, fine to medium-sized (1 to 3.5 mm), with polysynthetic twinning and compositional zoning, with cores altered to muscovite. Scarce sillimanite is included within plagioclase. Biotite occurs as subidiomorphic sheets, with pleochroism from light to dark brown in color. Apatite and zircon/monazite are found as accessory minerals, while muscovite, chlorite, rutile and sericite appear as alteration minerals. Muscovite forms coarse xenomorphic sheets partially replacing potassium feldspar, plagioclase, and quartz.

Pichanas migmatites

These rocks are gray, medium to coarse grain in size, with a coarse $\rm S_2$ foliation (Fig. 3g). Scarce potassium feldspar occurs as tabular to rounded porphyroblasts up to 2.5 cm long, white to pink in color, with two-individual twinning, and inclusions of quartz and biotite. Black tourmaline crystals (schorl) are also present. Biotite sheets anastomose around the porphyroblasts, collectively defining the foliation of the rock. In some areas, a very marked gneissic fabric is recognized.

At the microscopic scale, the texture (Fig. 7h) consists of three main components: (a) medium- to coarse-grained (< 4.5 mm) granolepidoblastic matrix composed of quartz, plagioclase, and potassium feldspar; (b) minor potassium feldspar porphyroblasts with irregular edges; and (c) dark bands composed of medium-grained lepidoblastic biotite. These bands anastomose around the potassium feldspar porphyroblasts, collectively defining the coarse S_2 foliation.

Quartz appears as coarse xenoblasts with lobate to sutured, bent edges and undulatory extinction, deformation bands, and chessboard extinction. In some sectors, it forms fine polygonal grains with triple junctions. In contact with potassium feldspar and plagioclase, it shows a string of beads texture. Plagioclase forms subidioblastic tabular to rounded grains, fine to medium in size, with straight to lobate edges and slight zoning. It contains inclusions of biotite, quartz, sillimanite, and zircon/monazite. Two-individual and polysynthetic twinning are present, with wedging and bending, kink bands displacing polysynthetic twins, and healed intragranular

fractures. In contact with potassium feldspar, a thin rim of different composition is observed. Locally, myrmekitic textures in contact with quartz and symplectic textures in contact with biotite and tourmaline are recognized.

Potassium feldspar appears as tabular to rounded blasts of variable size (2 to 25 mm), some poikilitic, with inclusions of biotite, quartz, sillimanite, and zircon/monazite. It exhibits grid twinning, bending, and diffuse twinning, undulatory extinction, and in some cases, rotated grains. At contacts with other minerals, it develops irregular edges. Biotite is subidioblastic, medium in size, and laminar to irregular in habit, with pleochroism from light brown to reddish dark brown. It is bent and shows kink bands. Tourmaline occurs as tabular to rounded fine grains (< 1 mm), with pleochroism from green to light yellow and symplectic textures in contact with quartz, plagioclase, and potassium feldspar. Accessory minerals commonly found are apatite, zircon/monazite and opaque minerals. The degree of alteration is low, to muscovite, green biotite, opaque minerals, rutile, and sericite.

MINERAL CHEMISTRY

The chemical compositions of the main mineral phases in the foliated porphyroblastic diatexites of La Totorilla, analyzed from a representative sample (#1017; Fig. 2), are provided in the Supplementary Material.

Potassium feldspar (n = 15 analyses) is xenoblastic, up to 4 mm long, exhibiting microperthitic texture and irregular albite patches, as well as rounded inclusions of plagioclase and quartz. Orthoclase content ranges between 86 and 93 %, while albite varies between 7 and 14 % (Fig. 8). The orthoclase content tends to decrease and the albite content to increase towards the rims; anorthite content is negligible.

Plagioclase (n = 15) is also xenoblastic and up to 2 mm long. A marked zoning is recognized, with a wide core and a thin rim (< 0.2 mm). Prismatic inclusions of sillimanite are recognized in the core, and quartz, potassium feldspar, and droplet-shaped biotite inclusions at the rims. The core composition is uniform and classified as oligoclase with 21–23 % anorthite, 76–79 % albite, and less than 1 % orthoclase (Fig. 8). At the rim, anorthite (16–20 %) and albite (69–73 %) contents decrease, while orthoclase increases significantly to 11 %, and is projected near the anorthoclase field.

Biotite (n = 12) appears as subidioblastic sheets up to 1 mm long, forming aggregates in the matrix, sometimes with quartz and feldspar symplectites. Some sheets are in contact with cordierite, while others correspond to replacement biotite, generally greener in color. In the annite–siderophyllite–

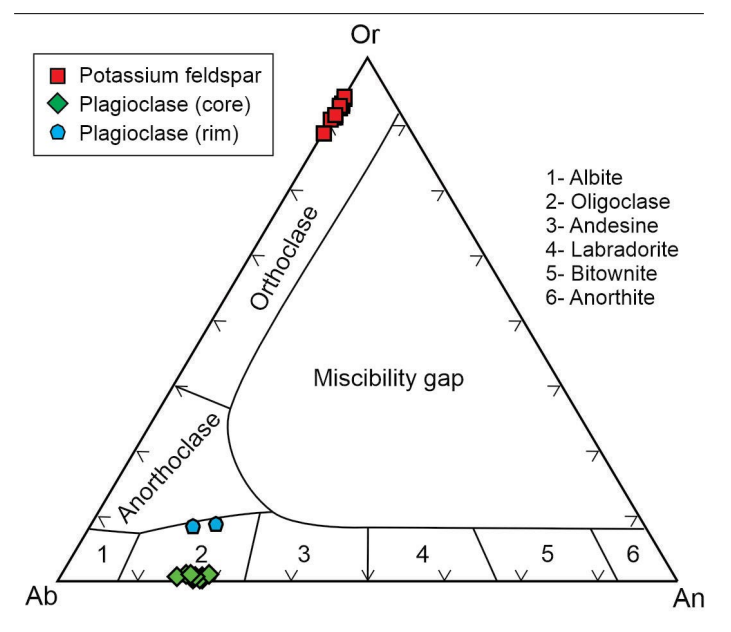


Figure 8. Ternary classification diagram of feldspars (Deer et al. 1963), showing the composition of potassium feldspar (n = 15) and plagioclase (n = 15) from the La Totorilla foliated porphyroblastic diatexites.

phlogopite-eastonite quadrilateral diagram (Fig. 9a; Speer 1984) for mica classification, the analyzed biotites show enrichment in siderophyllite with high Al^{IV} contents, ranging from 2.62 to 2.77 a.p.f.u. (22 O) in matrix biotites; 2.60-2.65 in those adjacent to cordierite; and lower values in green biotite (2.55). The Mg/(Mg+Fe) ratio varies between 0.46-0.50 in matrix biotites and 0.51-0.55 in those adjacent to cordierite and green biotite. Alvi contents are lower in matrix biotites (0.50-0.78) and higher in those adjacent to cordierite and green biotite (0.80-0.90 a.p.f.u.). TiO2 contents are relatively high in matrix biotites (average ~ 3 %), slightly lower adjacent to cordierite (average 2.25 %), and almost negligible in green biotite (0.26 %). Maximum fluorine content is 1.81 % in matrix biotite; 1.54 % adjacent to cordierite; and 1.07 % in green biotite. In the ternary TiO₂–FeO_T (= FeO + MnO)–MgO diagram (Nachit et al. 2005), matrix biotites plot mainly in the primary biotite field (Fig. 9b), those adjacent to cordierite tend toward reequilibrated biotites, and green biotite with very low TiO₂ clearly plots in the secondary biotite field.

Cordierite (n = 16) is xenoblastic, up to 2 mm long, slightly altered to pinite at edges and fractures. Its composition is fairly uniform, with Mg/(Mg+Fe) between 0.63 and 0.67. Na $_2$ O contents range from 0.27 to 0.41 %, while K $_2$ O is below 0.06 %. Although the fluid phase composition was not determined, low CO $_2$ contents are inferred due to the absence of graphite and calcite in the paragenesis. In the (Na+K) *versus* Mg/ (Mg+Mn+Fe $^{2+}$) classification diagram, based on data from multiple authors (Pereira and Bea 1994 and references therein), most analyses (12) fall within the anatectic cordierite

field, with a few (4) within the magmatic field (Fig. 9c). In the discriminant ($Na_2O + K_2O + CaO$) versus MnO diagram (Fig. 9d; Barbero and Villaseca 1992; Villaseca and Barbero 1994), all analyses plot within the metamorphic cordierite field (also including cordierite from anatectic leucogranites and restiterich granites from migmatite—granulite terrains), close to the boundary with igneous cordierites from S-type granites.

Muscovite (n = 7) occurs in scarce subidioblastic sheets up to 0.5 mm long, replacing biotite included within cordierite. It contains 9–12 % paragonite component; 2.8–3.4 % combined Fe, Mn, Mg, and Ti oxides, with 0.09 to 0.24 % TiO_2 . Another type, in very fine sheets (< 0.05 mm) associated with quartz and feldspar symplectites in biotite, has lower paragonite content (5 %) and higher TiO_2 (0.83 %). In the (Fe_t+Mg)–Al^{IV}–Al^{VI} diagram (Fig. 9e; Guidotti 1984) for white mica classification, both types plot between ideal muscovite and ferrimuscovite [theoretical formula: K(Al,Fe³+) $_2$ (AlSi $_3$ O $_{10}$)(OH) $_2$]. In the Mg–Ti–Na diagram (Fig. 9f; Miller et al. 1981), muscovite associated with symplectites plots in the primary white mica field, while replacement muscovite clearly falls in the reequilibrated or secondary white mica field.

No Fe–Ti oxides (magnetite–ilmenite) suitable for analysis were identified, except for very fine exsolutions along edges and cleavage planes of altered biotite.

GEOCHRONOLOGY

A total of 110 zircon grains from sample #1017, representative of the La Totorilla foliated porphyroblastic diatexites (Fig. 2a), were selected for analysis. In this sample, zircons are abundant, measuring 150 to 200 µm in size, with euhedral to subhedral shapes and colors ranging from pink to colorless. Many grains have rounded edges, and some are fractured. Most crystals (80 %) are elongated prismatic with length-to-width ratios of 4:1 to 6:1. A smaller proportion (20 %) consists of shorter crystals tending toward bipyramidal shapes with length-to-width ratios of approximately 2:1.

Eighty-one spots were analyzed on 80 zircon grains, preferentially at the rims to better constrain the metamorphic age. Of these, 70 data points exhibit high concordance (100 ± 10 %) and were used to calculate metamorphic and possible inherited ages. The U–Pb analytical data are presented in Table 2 and plotted on a Wetherill concordia diagram (Fig. 10a). The analyzed zircons have average uranium (238 U) contents of 1141 ppm (ranging from 51 to 5094 ppm) and thorium (232 Th) contents of 52 ppm (ranging from 8 to 584 ppm).

In 76 % of the total dataset (n = 53/70), the Th/U ratio is

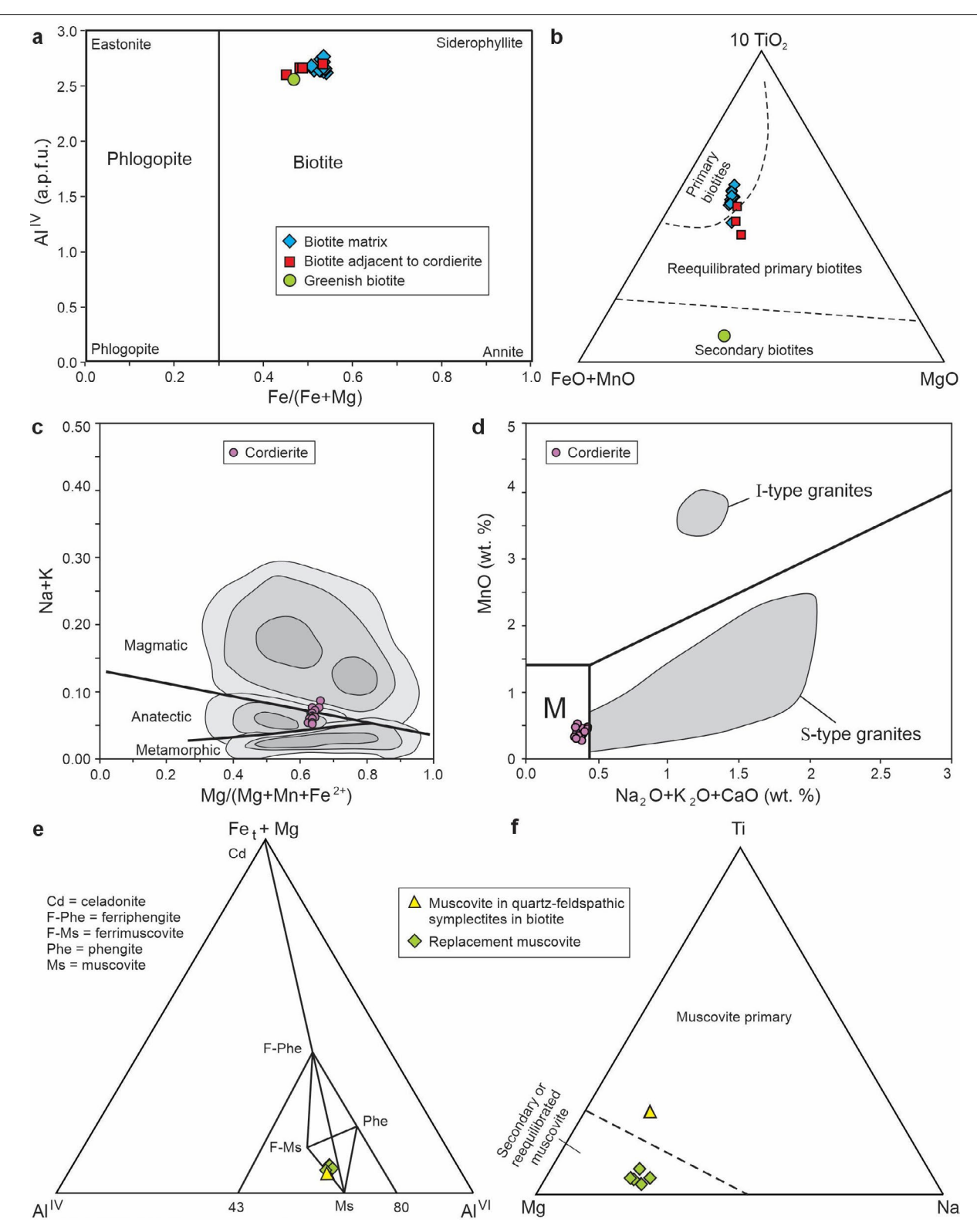


Figure 9. Mineral chemistry of the La Totorilla foliated porphyroblastic diatexites. (a–b) Classification of different biotite textural types (n = 12) in the Speer (1984) diagram and the ternary TiO_2 – FeO_7 –MgO diagram of Nachit et al. (2005), distinguishing primary, reequilibrated, and secondary biotites. (c) Composition of cordierite (n = 16) in the Na+K *versus* Mg/(Mg+Mn+Fe²+) diagram, based on data from multiple authors (Pereira and Bea 1994 and references therein), differentiating metamorphic, anatectic, and magmatic cordierite; shaded areas indicate data concentrations. (d) Discriminant diagram (Na₂O + K₂O + CaO) *versus* MnO showing compositional fields for metamorphic (M) and igneous cordierite (S- and I-type granites) according to Barbero and Villaseca (1992) and Villaseca and Barbero (1994). Field M includes cordierites from anatectic leucogranites and restite-rich migmatite–granulite terrains. (e–f) Muscovite classification (n = 7) in the (Fe₁+Mg)–Al^{IV} diagram (Guidotti 1984) and the Mg–Ti–Na diagram (Miller et al. 1981), distinguishing primary from secondary or reequilibrated white micas.

less than 0.1, typical of metamorphic zircons (Rubatto 2002, Hoskin and Schaltegger 2003), and is distributed in a range between 467 and 656 Ma. Data with Th/U ratios higher than 0.1, considered intermediate to typical of igneous zircons (Th/U > 0.3–0.5; Hoskin and Schaltegger 2003), have ages older than 527 Ma.

A kernel density estimation (KDE) diagram for the 70 concordant age data (Fig. 10b) shows a main peak at approximately 530 Ma, a secondary peak at \sim 480 Ma and two minor peaks at \sim 603 and \sim 636 Ma. Seven very minor age peaks are recognized at \sim 760, \sim 848, \sim 1015, \sim 1076, \sim 1159, \sim 1737, and \sim 2030 Ma.

To calculate the metamorphic peak age, the population data corresponding to the main peak in the KDE diagram and with Th/U ratios less than 0.1 was selected. For this dataset, ranging between 519 to 548 Ma (n = 24/70), a concordia age of 532.1 \pm 1.7 Ma was obtained (Fig. 10c).

STRUCTURE

The outcrops and rocks described in this study are located within the footwall block of the La Higuera fault (Fig. 2a), which strikes N 310° and dips 40° to the northeast. This block, extending from northeast to southwest, encompasses the La Higuera–Dos Pozos ductile shear zone (Sureda 1978, Martino 2003) and the Pichanas migmatites. The latter include the La Totorilla foliated porphyroblastic diatexites and the biotite monzogranite body, most of which contain xenoliths derived from the Tuclame Banded Schists and biotite gneisses.

It is important to note that, except for the Pichanas migmatites (the most abundant rock type in the area), all recognized lithologies (diatexites, monzogranite, and xenoliths) outcrop as lenticular bodies. These bodies are arranged as boudins of varying sizes, from decimeters to hundreds of meters in length, with an average neck orientation of N 230°/75° (Fig. 2a, b). Following the classification of Goscombe et al. (2004), these structures correspond to symmetric drawn boudins.

The main penetrative structure recognized in all rocks of the area (Fig. 2a, b) is a metamorphic foliation, designated S_2 (see below, Interpretation of the Structure Section). In the Pichanas migmatites, the S_2 foliation is defined by the orientation of biotite sheets and potassium feldspar porphyroblasts. It is also marked by the orientation of lenticular xenoliths, whose principal direction is parallel to S_2 (Fig. 3g). In the La Totorilla diatexites, the S_2 foliation is marked by the orientation of biotite, sillimanite, and elongate blasts of quartz and cordierite, which anastomose around potassium feldspar porphyroblasts oriented in the same direction (Fig.

3b). These porphyroblasts exhibit characteristic morphology and orientation in two sections perpendicular (XZ and YZ, XYZ: principal finite strain axes) and one parallel to S_2 (XY), defining the mesoscopic fabric of the diatexites (Fig. 4a–c). In sections perpendicular to S_2 , feldspars have tabular shapes, irregular edges, and simple twins. In sections parallel to S_2 , porphyroblasts become flattened or oblate with irregular edges, resembling a "torreja" (= french toast) morphology (Fig. 11b). In the biotite monzogranite, the S_2 foliation is poorly defined, marked by the preferred orientation of biotite. Field data indicate that the S_2 foliation in all mentioned lithologies has an average strike of N 300°, with dips varying from 55° to vertical (90°), dipping both southwest and northeast. These values scatter along a fabric axis N 300°/20° (Fig. 11a), giving a high-angle, fan-shaped foliation in section A–A' (Fig. 2b).

Lineations are very scarce in the study area (only two measurements, Fig. 11a). Mineral lineations associated with the $\rm S_2$ foliation plane have been found in the Pichanas migmatites (N 290°/20°) and La Totorilla diatexites (N 250°/48°), marked by biotite alignment. These lineations scatter in a great circle oriented N 304°/56° SW. Roughly, the $\rm <c>$ axis orientation of potassium feldspar porphyroblasts in La Totorilla diatexites ranges between N 290° and N 330°, mainly visible in the XZ section parallel to the erosive horizontal surface.

Regarding lenticular xenoliths, in the Pichanas migmatites their long axis is parallel to the S₂ foliation (Fig. 3g), the intermediate axis is parallel to the foliation dip, and the short axis is perpendicular to it. The contact between migmatites and xenoliths is sharp; locally, leucosomatic material in the form of veins is present within the xenoliths. These are variably fragmented, reaching an advanced state as biotite schlieren parallel to the S₂ foliation in the migmatites. The xenoliths within the La Totorilla diatexites are oriented in the same way as within the Pichanas migmatites but show a different relationship at the contact. Here, mullions (Sokoutis 1990, Martino 2009) are recognized, with their symmetrical and asymmetrical cusps pointing towards the diatexites, while towards the ends the contact is interdigitated (Figs. 3c, d and 11b). The xenoliths are also dismembered in the form of biotite schlieren parallel to the S₂ foliation.

Tourmaline-bearing granitic veins (pegmatoids), ranging from centimeter to decimeter scale, cut across the Pichanas migmatites and La Totorilla diatexites. They occur in three types (Fig. 11a): (a) intensely deformed, lenticular veins, parallel to the dominant S_2 foliation (boudins); (b) folded veins, with intensities varying from gentle folds to nearly intrafolial folds, the latter with an axial planar cleavage coincident with S_2 (Fig. 3f); and (c) undeformed veins, oriented N 20°/90°, cutting across the S_2 foliation plane.

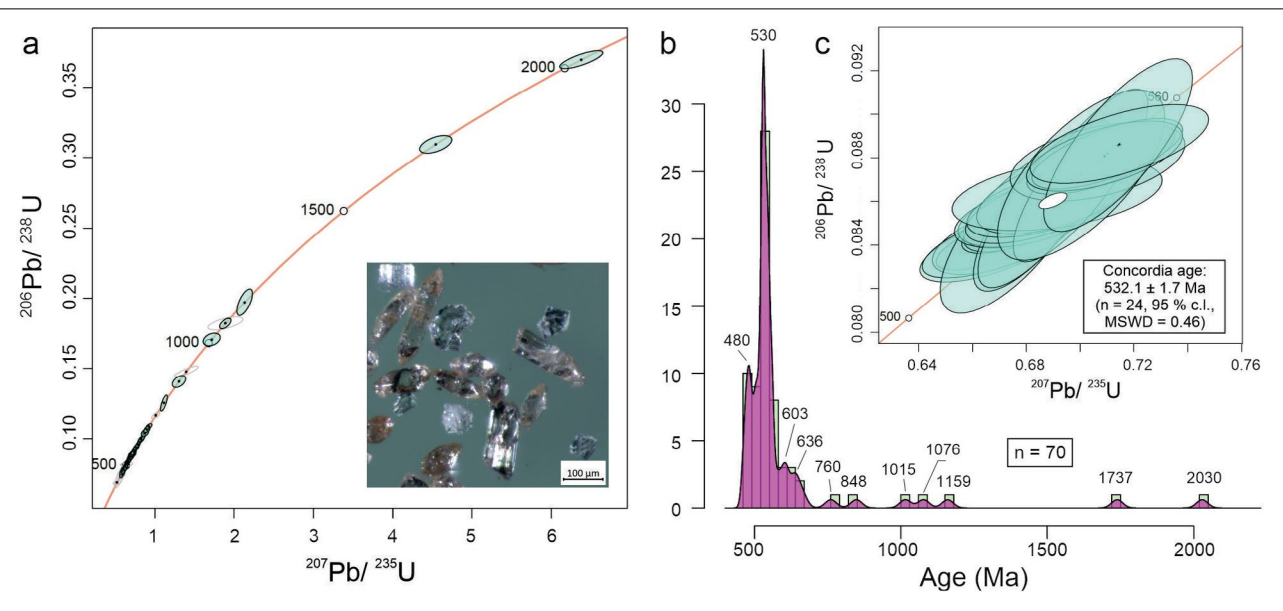


Figure 10. U–Pb data of zircon grains, preferentially at the rims, from sample #1017 of the La Totorilla foliated porphyroblastic diatexites. (a) Wetherill concordia diagram for 81 data point (70 concordant). All error ellipses are at 95 % confidence; gray ellipses indicate data excluded due to > 10 % discordance. The photomicrograph shows shapes and colors of some grains before selection, mounting, and polishing. (b) Kernel density estimation (KDE, bandwidth: 7.5 Ma) and histogram (binwidth: 50 Ma) showing the distribution of 70 data points, excluding > 10 % discordant data. (c) Wetherill concordia diagram for 24 data points corresponding to the main peak in the KDE diagram and with Th/U ratio < 0.1. All error ellipses are at 95 % confidence

In the La Totorilla diatexites, three orthogonal joint sets are recognized (Fig. 11a): two subvertical, trending northwest (N 280°/80° NE) and north (N 355°/90°), and one subhorizontal. These structures are used for the quarrying of diatexites as application rocks.

In a sector of the Pichanas migmatites, the La Higuera–Dos Pozos ductile shear zone (Fig. 2a, b) overprints the rocks, with a mylonitic foliation oriented N 310°–320°/60° NE and a stretching lineation on this plane oriented N 110°/40–50° (Fig. 11a). Kinematic indicators show a general reverse sense with a subordinate sinistral strike-slip component (Martino 2003).

PRESSURE-TEMPERATURE ESTIMATES

The physical conditions of metamorphism and deformation in the La Totorilla foliated porphyroblastic diatexites were estimated based on the chemical composition of minerals, observed textures, and microstructures.

Because garnet is absent, it was not possible to apply garnet—biotite or garnet—cordierite thermobarometers. Similarly, the lack of ilmenite or rutile associated with biotite precluded the use of the Ti-in-biotite thermometer. Consequently, peak metamorphic temperatures were estimated using the Na-in-cordierite thermometer, which is relatively insensitive to pressure. The experimental calibration of Trooper et al. (2018) for cordierite in equilibrium with plagioclase was employed. The obtained temperatures yield

an average of 788 \pm 15 °C, ranging from 745 to 817 °C (see Supplementary Material).

The presence of stable cordierite in the peak metamorphic paragenesis, with an average Mg/(Mg + Fe) ratio of 0.65, and the absence of garnet allow to estimate that the pressure was equal to or less than 6 kbar, for a temperature range of 700–800 °C (Currie 1971).

Taking into account the maximum pressure found (P \approx 6 kbar), which we assume as the lithostatic pressure (P_L), the maximum depth (z) at which the La Totorilla diatexites were generated can be estimated (e.g. Nicollet 2010, Yardley and Warren 2021). Using a classical model —without considering tectonic stresses—through the formula z = P_L/pg, where ρ = 2.7 × 10³ kg/m³ (average density of the continental crust) and g = 9.8 m/s² (acceleration of gravity), the maximum value of the depth (z) is approximately 22 km, which corresponds to the middle part of a crust of 35-40 km in total (Perarnau et al. 2012).

Regarding textural relationships, lobate-cuspate intergrain contacts between quartz and feldspars (both plagioclase and potassium feldspar, Figs. 6 and 7) are observed, resulting from the crystallization of a granitic melt (Vernon 2001). The estimated temperature for this crystallization, according to experimental data from Díaz Alvarado (2017), would be 700–750 °C. During the generation and crystallization of this melt, and associated with deformation, microboudinage of sillimanite prisms likely occurred (Fig. 6b), which remain as relics along with biotite within plagioclase and potassium

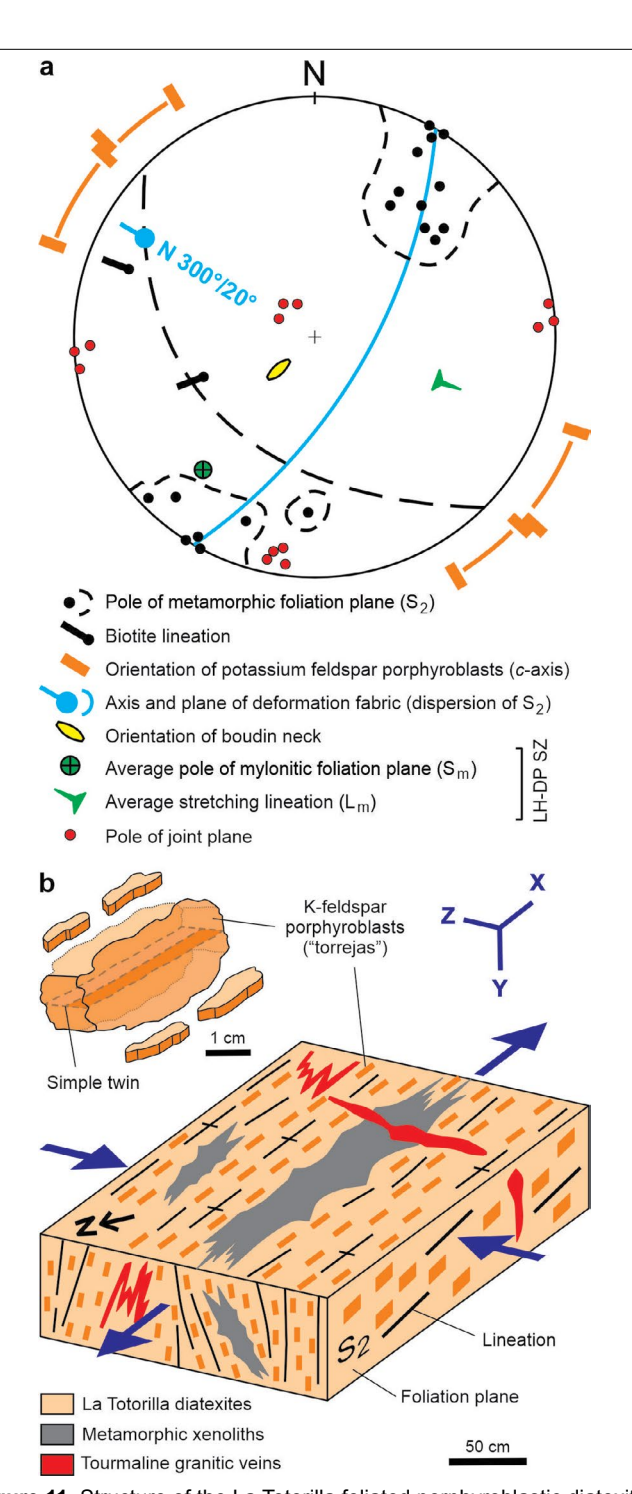


Figure 11. Structure of the La Totorilla foliated porphyroblastic diatexites. (a) Stereographic projection (lower hemisphere Schmidt net) of structural elements measured in the La Totorilla foliated porphyroblastic diatexites and associated rocks. LH–DP SZ: La Higuera–Dos Pozos shear zone. (b) Block diagram showing the relationship between fan-shaped S_2 foliation, potassium feldspar porphyroblasts, biotite lineation, deformed metamorphic xenoliths with mullion contacts having symmetric and asymmetric cusps pointing toward the diatexites and interdigitated at the ends, and tourmaline-bearing granitic veins with varying degrees of deformation. Arrows indicate shortening (finite strain axis Z, perpendicular to S_2) and stretching (X, parallel to S_2) directions. Detail of potassium feldspar porphyroblast morphology, with tabular habit in ZX and ZY sections, irregular oblate shapes in XY, and two-individual twins with $\langle c \rangle$ axis parallel to X in XZ.

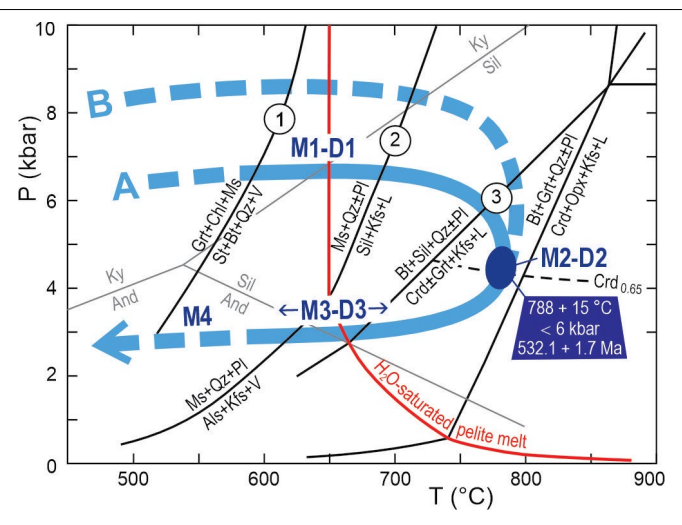


Figure 12. Pressure–temperature diagram showing the inferred clockwise P-T path for the La Totorilla foliated porphyroblastic diatexites (A), deformation, and timing of the metamorphic peak. Based on the petrogenetic grid of Spear et al. (1999) for anatexis of metapelites in the NaKF-MASH system, with sufficient sodium to stabilize albite and water generated by dehydration melting reactions. V: vapor. L: liquid. $Crd_{0.65} = Mg/(Mg + Fe)$ in cordierite in divariant assemblages. The P-T path (B) proposed for the San Carlos Migmatitic Massif and Yacanto Group (Martino et al. 1997, 2005; Guereschi and Martino 2008, 2014) is included for regional comparison.

feldspar produced by anatexis (Fig. 12).

The microstructures identified in the rocks of the study area reflect post-crystalline plastic deformation and provide constraints on the temperature conditions during their formation:

- (a) In quartz, features such as chessboard extinction (Fig. 7b, resulting from dislocation glide along (a) and (c) axes), mantle and core texture (grain size reduction, grain boundary migration, and recrystallization), and polygonal granoblastic aggregates (recrystallization) interstitial to feldspars, indicate deformation at high temperatures (> 650 °C; Kruhl and Hunteman 1991). In sillimanite, the formation of fibrolite, associated with shear deformation along the basal plane of biotite (Fig. 5a,b), would also fall within this temperature range.
- (b) In plagioclase, polysynthetic twinning with wedging and bending, and undulatory extinction, suggest deformation at temperatures of 500–400 °C (Passchier and Trouw 2005). Similar conditions are assigned to potassium feldspar, which shows deformed twins and undulatory extinction (Figs. 6a, d, and 7a, c).
- (c) Other features, such as quartz stretched parallel to the $\rm S_2$ foliation with deformation bands (Fig. 5b), and biotite that is bent, with ragged edges and kink bands (Fig. 7c, d), suggest lower temperature conditions (< 400 °C). The pinitization of cordierite could also be considered within this temperature range (Figs. 5a, b, and 7e). Under these conditions, the microkink bands observed in potassium feldspar (Fig. 7a, c)

were probably also formed.

TEXTURAL EVOLUTION AND PRESSURE-TEMPERATURE PATH

The La Totorilla foliated porphyroblastic diatexites exhibit mineral associations and textures that reflect a state out of equilibrium both from a petrological and structural perspective. Various paragenetic associations and metamorphic reaction textures were identified in these rocks, occurring in both solid-state and partial melting conditions, typical of a pelitic protolith, along with a variety of deformational microstructures formed at different temperatures. These features can be grouped into three main stages of metamorphic evolution: a first, prograde stage of relic character; a second, peak-metamorphic stage involving anatexis and deformation; and a retrograde stage marked by continued deformation, cooling, and final hydration of the system. Mineral abbreviations follow Whitney and Evans (2010).

Prograde stage

The presence of inclusions of quartz, plagioclase, biotite, and particularly staurolite (Fig. 6b) within minerals such as potassium feldspar, plagioclase and quartz, are attributed to a medium-grade (M1) metamorphic event of the prograde stage. The relict paragenesis of this event is given by: (I) $Qz_1 + Pl_1 + Bt_1 + St \pm Ms_1$.

The biotite + staurolite association [reaction (1) in Fig. 12] appears at temperatures around 600 °C and marks the onset of the mid-amphibolite facies, within a variable medium-pressure range (Bucher and Frey 1994). The probable presence of zinc in staurolite could explain its persistence at high grade conditions (Ashworth 1975).

Although primary muscovite (Ms₁) was not detected, it is assumed to have been initially present as part of the M1 paragenesis, likely associated with a deformation event D1, and completely consumed during progressive metamorphism.

Metamorphic peak

The highest-grade paragenesis recognized for the metamorphic peak M2 in the La Totorilla diatexites is: (II) $Qz_2 + Bt_2 + Pl_2 + Sil + Kfs + Crd$. This paragenesis (Fig. 5a, b) indicates that conditions well beyond the sillimanite + potassium feldspar zone were reached, and that muscovite disappearance occurred via the reaction marking the onset of high-grade metamorphism (Spear et al. 1999): (2) Ms + $Qz \pm Pl = Sil + Kfs_1 + melt_1$, probably giving rise to stromatic metatexites with quartz–feldspathic leucosomes (Fig. 3e).

After surpassing reaction (2), near-isobaric heating would have reached equilibrium conditions for the dehydration

melting reaction of biotite (Bucher and Frey 1994): (3) Bt + Sil + Qz \pm Pl = Crd \pm Grt + Kfs $_2$ + melt $_2$. This reaction produces cordierite and/or garnet depending on pressure. Garnet was not found in La Totorilla diatexites, suggesting pressure was less than or equal to 6 kbar. The estimated average temperature for the M2 metamorphic peak is 788 \pm 15 °C, based on the sodium-in-cordierite thermometer (Trooper et al. 2018, Supplementary Material). These conditions correspond to cordierite stability in the presence of potassium feldspar and melt during the development of reaction (3), an incongruent vapor absent melting reaction.

Textural evidence for reaction (3) includes corroded and ragged biotite sheets in contact with both potassium feldspar and cordierite, with melt films forming along edges and quartz–feldspar symplectites (Figs. 7c, d, e). These prominent features reflect the destabilization of biotite and its decomposition to act as a source of elements for the just mentioned minerals. Sillimanite also likely participated as a reactant, in addition to biotite, since both minerals remained as relict inclusions within cordierite, potassium feldspar, and plagioclase formed by the anatectic (3) reaction (Fig. 6a, b, c and 7f). All reactants would have been in excess, since biotite and even sillimanite remain in the matrix (Figs. 5a, b).

Other textural features indicative of *in situ* partial melting, according to criteria by Holness (2008), Holness et al. (2011), and Vernon (2011), include: lobate contacts with low dihedral angles between reaction products (cordierite, potassium feldspar, plagioclase, and quartz; Figs. 6c, e, f and 7a, b, c, e); aligned potassium feldspar porphyroblasts with simple twinning (Figs. 3b and 6a); string of beads texture of quartz and plagioclase in potassium feldspar, produced when melt concentrated in grain boundary films (Figs. 6d and 7a); and droplet-shaped biotite inclusions within the main minerals.

Simultaneously with the M2 metamorphic peak, the penetrative $\rm S_2$ foliation developed (Figs. 3b and 5a, b), associated with the deformation event D2, represented by the oriented growth and/or recrystallization of minerals defining the rock.

Retrograde stage

This stage, associated with a deformation event D3, mainly involved textural changes (M3). The identified textural evidence includes fibrolitization of sillimanite and post-crystalline deformational microstructures in the minerals (Fig. 7a, b, d). Among these, other notable features are: undulatory extinction in a chessboard pattern and in deformation bands, grain boundary migration, and formation of smaller polygonal grains in quartz; undulatory extinction, wedging, bending, and blurring of polysynthetic twinning in plagioclase; undulatory

extinction, blurred twinning, and flame perthitic textures in potassium feldspar; bending, undulatory extinction, and kink bands in biotite. Deformation likely began immediately after the metamorphic peak, with the mineral assemblage already in the solid state, at temperatures above 650 °C, and continued down to temperatures below 400 °C.

As the final part of the retrograde stage, system hydration likely occurred, with alteration processes under low-grade metamorphic conditions during an event M4. These include the formation of secondary muscovite (Ms_2), sericitization and kaolinization in plagioclase and potassium feldspar, pinitization and sericitization in cordierite, and formation of green biotite associated with biotite and cordierite (Figs. 5a, b and 7f). The development of some of these minerals can be attributed to the following retrograde reaction: (4) Kfs + Crd + H_2O = Bt (green) + Ms_2 + Qtz (Bucher and Frey 1994).

Pressure-temperature path

The mineral paragenesis, reaction textures and deformation microstructures recognized at different stages of evolution allow us to deduce that the pressure–temperature (P-T) path followed by the La Totorilla foliated porphyroblastic diatexites formed a clockwise loop (A in Fig. 12) in the petrogenetic grid of Spear et al. (1999). This grid is valid for the anatexis of metapelitic rocks in the NaKFMASH system, with sufficient sodium to stabilize albite and where the only available water is generated by dehydration melting reactions.

During the prograde stage, the path passed through medium-grade conditions [reaction (1)], within the stability field of staurolite + biotite. During a regional metamorphic event M1–D1, muscovite was likely associated with the paragenesis. Physical conditions of approximately 600 °C temperature and 6 kbar pressure are estimated for M1.

At the M2 metamorphic peak, associated with nearisobaric heating, the path surpassed reaction (2) involving muscovite + quartz breakdown, initiating partial melting or anatexis in metapelitic rocks, probably giving rise to stromatic metatexites. With further temperature increase, reaching high-grade metamorphic conditions in the biotite dehydration melting reaction (3), a high percentage of melts was generated, giving rise to the La Totorilla diatexites. Concurrently, the S_2 metamorphic foliation developed during the deformation event D2. Estimated conditions are 788 ± 15 °C (based on the sodium-in-cordierite thermometer) and pressures equal to or less than 6 kbar, with generation of cordierite [Mg/(Mg + Fe) = 0.65] + potassium feldspar + melt (without garnet).

During the retrograde stage, event M3–D3, the postmetamorphic deformation microstructures described in previous sections developed progressively. From this point, all lithologies in the area likely followed a common retrograde path from medium to low temperature (M4), with hydration and formation of alteration minerals.

In summary, the clockwise *P*–*T* path inferred for the La Totorilla foliated porphyroblastic diatexites records an evolution that began under medium-grade conditions, followed by a high-grade metamorphic peak with partial melting and progressive deformation, and culminated in a stage of cooling and alteration.

INTERPRETATION OF STRUCTURE

In addition to the localized La Higuera–Dos Pozos ductile shear zone, the main structure in all of the rocks of the studied area (Fig. 2a) is the penetrative S_2 metamorphic foliation, designated S_2 by regional correlation with rocks of the rest of the San Carlos Migmatitic Massif (Martino and Guereschi 2014 and references therein). This foliation affects the La Totorilla foliated porphyroblastic diatexites, the biotite monzogranite and the Pichanas migmatites and is expressed in several particular features:

- (1) Ellipsoidal shape of the bodies at map and outcrop scale: both the La Totorilla and the biotite monzogranite bodies are ellipsoidal, with their major axis parallel to S_2 (Fig. 2a). Metamorphic xenoliths also have ellipsoidal shapes, often dismembered to form biotite *schlieren* parallel to S_2 (Fig. 3c, d, e, g). The type (a) granitic veins also show a lenticular shape.
- (2) Orientation and morphology of feldspars: the potassium feldspar porphyroblasts are flattened (oblate geometry in the XY section, Fig. 4b) in the direction of the S_2 foliation.
- (3) Scarcity of lineations: lineations associated with the S_2 foliation are rare and scattered along a great circle (Fig. 11a), indicating that deformation was mainly by flattening.

This set of features is interpreted as the product of penetrative deformation with flattening perpendicular to the $\rm S_2$ foliation plane and stretching parallel to it, in a pure shear regime. This penetrative deformation likely began simultaneously with the M2 metamorphic peak, under the same high-temperature and partial melting conditions that generated the La Totorilla diatexites. The orientation of minerals along the $\rm S_2$ foliation plane (mainly potassium feldspar, biotite, and elongate quartz) reflects the anisotropic stress field during syn-migmatitic recrystallization.

At both map and outcrop scale (Figs. 2a and 11b), flattening deformation caused symmetric boudinage of the La Totorilla body, the biotite monzogranite body, the metamorphic xenoliths, and the type (a) granitic veins within the Pichanas migmatites (Fig. 3g). These symmetric drawn boudins indicate

ductile behavior and low competence contrast among the rocks, with Pichanas migmatites being the most deformable. In contrast, xenoliths within the La Totorilla diatexites display mullion (festooned) structures at their edges, with cusps perpendicular to the S_2 foliation plane (Figs. 3c, d and 11b). This suggests that, in this case, the diatexites were more competent (resistant to deformation) than the xenoliths, which is not typically expected in a partially molten rock. A possible explanation is that the diatexites are rich in potassium feldspar, while the xenoliths are rich in quartz; feldspars may impart greater rigidity to the diatexites, despite partial melting. Notably, the La Totorilla body was boudinaged within the Pichanas migmatites, indicating that La Totorilla was more rigid than Pichanas (Fig. 2a, b).

Pure shear deformation likely continued after rock consolidation, as evidenced by the progressive folding of tourmaline-bearing granitic veins (Fig. 3f). These veins and the tourmaline-rich biotite monzogranite body probably represent a late stage, associated with crystallization of volatile-rich melts after the main anatexis event (M2). Structurally, during D2–D3 events, the veins evolved from type (a) boudins to intrafolial folds, and finally to late open to gentle folds in type (b) veins. This deformation also affected the Pichanas migmatites, imparting a gneissic fabric in some areas, such as was observed in the southwestern contact of the La Totorilla anatectic body.

Post-crystalline microstructures show progressive deformation from high temperature (chessboard extinction in quartz, microboudinage in sillimanite, wedged twinning in plagioclase) to lower temperature (fibrolite development, kink bands in biotite). Finally, undeformed type (c) tourmaline-bearing granitic veins were emplaced.

In summary, the $\rm S_2$ foliation penetrative in all lithologies of the studied area is the result of a complex evolution involving metamorphism, anatexis, and flattening deformation. Deformation diminished over time, with decreasing temperature, shifting from intense to weaker flattening, as seen in the granitic veins and microstructures. This progressive deformation affected all rocks, resulting in the $\rm S_2$ foliation with a N 300–330° orientation and a simple appearance observed in the field.

At the mesoscopic scale, in addition to the $\rm S_2$ foliation, another notable feature used in the naming of the La Totorilla diatexites is the size of the potassium feldspar that forms porphyroblasts up to 5 cm long (Figs. 3b and 4). The growth of large potassium feldspar crystals would have been facilitated by high temperature (750–800 °C) and the high melt fraction typical of diatexites, with possible potassium enrichment from melting of micaceous materials (paleosome remnants

represented by the xenoliths), in addition to biotite being the main reactant. Dynamic crystallization conditions under pure-shear deformation, together with the presence of aqueous migmatitic fluids, also promoted the prolonged growth of porphyroblasts.

Zoning in potassium feldspar porphyroblasts (mainly marked by aligned biotites, Fig. 4b, c) suggests an early stage of euhedral crystal growth, with two-individual twinning, in a melt-rich environment (Moore and Sisson 2008, Díaz Alvarado 2017). This was followed by a late stage of blastesis or growth in the solid state, probably with higher sodium content and perthite formation. These potassium feldspar rims had irregular, amoeboid, and interstitial edges toward the matrix reactant minerals (quartz, plagioclase, biotite, and sillimanite), which remained as inclusions (Fig. 6a, b, c). The dynamic environment also favored recrystallization of pre-existing feldspar crystals, which dissolved and reprecipitated as larger grains elongated along the foliation (Silva et al. 2023).

DISCUSSION

At first glance, the characteristics of occurrence, composition, and the presence of xenoliths suggest that the La Totorilla body could be classified as a "porphyritic granitoid" (Figs. 3b and 4). However, detailed petrographic analysis reveals evidence of metamorphic and partial melting processes that are not typical of igneous rocks crystallized directly from a magma. This evidence, along with the involved petrogenetic processes, indicate that it is a metamorphic rock of an anatectic origin. Delicate textural features, such as lobate-cuspate contacts between quartz, plagioclase and potassium feldspar, as well as corroded and ragged biotite sheets in contact with potassium feldspar and cordierite, with formation of melt films along the edges and quartz-feldspar symplectites, indicate extensive in situ partial melting and melt precipitation (Figs. 6 and 7). These textures have been preserved despite subsequent deformation, supporting their classification as diatexites —a type of migmatite characterized by a high proportion of melt material. Furthermore, the chemical composition of cordierite, a common mineral in these rocks, indicates a metamorphic-anatectic rather than magmatic origin (Figs. 9c, d). The rocks are also characterized by the development of large potassium feldspar crystals (megaporphyroblasts) and a coarse planar S_2 foliation, justifying their classification as foliated porphyroblastic diatexites (Figs. 3b and 4).

In the foliated porphyroblastic diatexites of La Totorilla, the abundance of potassium feldspar and aluminum-rich minerals

such as sillimanite and cordierite suggests a high aluminum content, indicating derivation from partial melting of pelitic or clay-rich greywacke sediments. In contrast, the Pichanas migmatites likely originated from a less aluminous, more sandy quartz-feldspathic protolith.

Despite the marked lithological contrast between La Totorilla diatexites and Pichanas migmatites, both rocks contain the same types of xenoliths (derived from the Tuclame Banded Schists and biotite gneisses), suggesting a genetic relationship between them. Under current exposure conditions, the La Totorilla body appears as a large boudin within the Pichanas migmatites (Fig. 2a, b). At first glance, this could be interpreted as an intrusive relationship, albeit with strong subsequent deformation. However, textural evidence of in situ partial melting in La Totorilla, such as the presence of crystallized melt "pools" and discrete quartzfeldspar leucosomes, indicates limited melt migration, favored by deformation under a pure shear regime. The high proportion of potassium feldspar relative to plagioclase and quartz suggests that a kind of matrix collapse and/or pressure filtration may have occurred, removing some of the melt richer in quartz and plagioclase and enriching the rock in potassium feldspar (cf. Sawyer 1994, 1991; Brown 1994; Vanderhaegue 2001; Silva et al. 2023).

One hypothesis to explain the observed relationships is that both La Totorilla diatexites and Pichanas migmatites coexisted in a high-ductility environment, transitioning into a metamorphic complex represented by the Tuclame Banded Schists and biotite gneisses. The latter would have remained as aligned xenoliths within the former lithologies, interpreted as paleosome remnants and restites (Mehnert 1968, Sawyer 2008b). The entire lithological assemblage would have been intensely deformed by flattening, with relative mobility between bodies of contrasting lithology and rheology. In this way, the La Totorilla body would have remained as a large boudin within the Pichanas migmatites (Fig. 13). The pronounced dip of the $\rm S_2$ foliation suggests that the La Totorilla diatexites could extend to greater depth.

The clockwise *P-T* path (A in Fig. 12) inferred for the La Totorilla foliated porphyroblastic diatexites indicates that, at the metamorphic peak (M2), cordierite, potassium feldspar, and a melt were formed by dehydration melting of biotite. The absence of garnet suggests that pressures were not high enough to stabilize it. An alternative explanation could involve variation in the composition of the protolith, because the crystallization of garnet in Mg-rich metapelites may be limited by the Fe/(Fe+Mg) ratio (Currie 1971, Bucher and Frey 1994). However, studies in the nearby Rumi Huasi migmatites (Lescano 2019), located 2 km southwest of La Totorilla (Fig.

2a), have identified small garnet relics within plagioclase, indicating these rocks also recorded a prior higher-pressure event. Furthermore, farther south in the San Carlos Migmatitic Massif, in the Juan XXIII and Río Hondo areas (Martino et al. 1997, 2005), garnet is a common mineral, although sometimes consumed by decompression reactions (plagioclase or cordierite coronas). This suggests that the anatectic rocks of La Totorilla may have undergone a previous higher-pressure stage with garnet presence, for which no textural evidence has yet been found. Under this alternative hypothesis, the P-T path of La Totorilla diatexites (denoted B in Fig. 12) would imply that the M2 metamorphic peak reached temperatures of ~ 800 °C and higher pressures of ~ 7.5-8 kbar (Martino et al. 2005), generating garnet, potassium feldspar, and melt. Then, during a decompression and cooling event, plagioclase would have completely consumed the garnet, leaving no relics in La Totorilla but preserving them in nearby migmatitic areas such as Rumi Huasi (Fig. 2a; Lescano 2019). This hypothesis implies pressures could have exceeded the 6 kbar estimated here, consistent with the known evolution of migmatites in the Sierras Pampeanas of Córdoba (Guereschi and Martino 2014 and references therein).

The La Totorilla body can be related to other anatectic bodies of the San Carlos Migmatitic Massif that have been well studied and show similar petrographic characteristics. The Juan XXIII diatexites (southeastern sector of the San Carlos Migmatitic Massif, Fig. 1) show a high-grade paragenesis of quartz + plagioclase + biotite + garnet + sillimanite + potassium feldspar at the metamorphic peak, with temperatures of 750 °C and pressures of 7.4 kbar, followed by cordierite formed by decompression during a retrograde stage, under conditions of 570-630 °C and 4.4-3.1 kbar (Martino et al. 2005). In the northeastern sector of the San Carlos Migmatitic Massif (Fig. 1), the El Pilón Granitic Complex (cordieritic granitoids and cordieritites, Gordillo 1984, Rapela et al. 2002) is hosted by cordierite diatexites and metatexites, with a paragenesis of quartz + plagioclase + biotite + potassium feldspar + sillimanite + cordierite, in addition to restitic material with garnet in the cordieritites. Rapela et al. (2002) determined conditions of 780 °C and 5.9 kbar for the melting event of the granitic source and conditions ranging from 650 \pm 16 °C - 3.3 \pm 0.3 kbar to 555 ± 52 °C $- 3.3 \pm 0.6$ kbar for the final emplacement of the granitoids.

Another important aspect to consider is those related to the internal structure of the main lithologies that constitute the San Carlos Migmatitic Massif. In particular, it is noted that the flattening deformation (pure shear) found in the La Totorilla foliated porphyroblastic diatexites clearly differs from the simple shear deformation found in most of the Massif, as

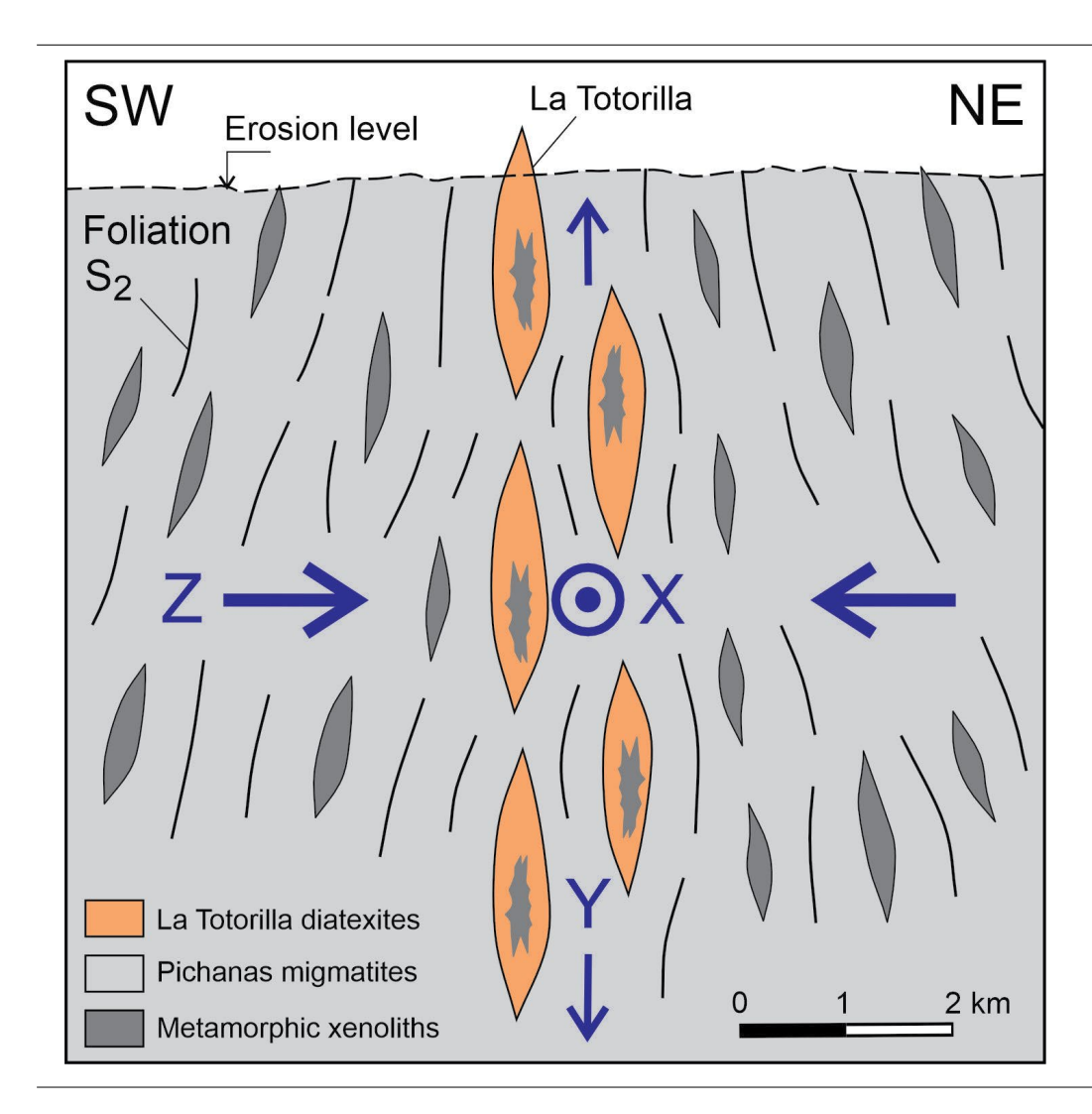


Figure 13. Interpretative schematic section of the La Totorilla anatectic body interlayered within the Pichanas migmatites, both lithologies in a high-ductility environment with aligned xenoliths derived from the Tuclame Banded Schists and biotite gneisses as paleosome remnants. All the lithologies were intensely deformed by flattening (pure shear, XYZ: principal finite strain axes), with relative mobility between bodies of contrasting lithology and rheology, leaving the La Totorilla body as a large boudin within the Pichanas migmatites. The high dip suggests the possible existence of more La Totorilla boudins at depth.

occurs in the well-studied areas of Río Hondo and Juan XXIII (Martino et al. 1997, 2004), among others.

Regarding geochronology, the dataset of zircon ages from the La Totorilla diatexites captures a protracted history common in complex terrains like those formed by migmatites. The seven very minor age peaks in the KDE diagram (Fig. 10b), at ~ 760, ~ 848, ~ 1015, ~ 1076, ~ 1159, ~ 1737, and ~ 2030 Ma, can be attributed to the presence of inherited zircons in the sedimentary protolith. These data points have Th/U ratios greater than 0.1, considered intermediate to typical of igneous zircons (Th/U > 0.3-0.5; Hoskin and Schaltegger 2003). The two minor peaks of zircon ages ~ 636 and ~ 603 Ma in the KDE diagram (Fig. 10b), most of them typically metamorphic (Th/U ratios < 0.1; Rubatto 2002, Hoskin and Schaltegger 2003), could be assigned to relicts of early stages of the Pampean orogeny, coincident with the late events of the Brazilian Collage (Brito Neves and Fuck 2013, Guereschi and Martino 2014).

The initial prograde stage of medium metamorphic grade (event M1–D1) in the La Totorilla diatexites would not have

been recorded as an age peak in the geochronological data. However, it would have been recorded in nearby areas, in rocks of regional distribution that can be correlated with those found as xenoliths within the La Totorilla diatexites, such as biotite gneisses (561 ± 10 , Sims et al. 1998) and the Tuclame Banded Schists. The latter are correlated with analogous rocks of the Conlara Complex in the Sierra de San Luis (564 ± 21 , Pb/Pb leaching experiments PbSL, Siegesmund et al. 2010).

The main age peak of ~ 530 Ma in the KDE diagram (Fig. 10b) would correspond to the high-grade M2–D2 metamorphic event, with anatexis and melt generation, that gave rise to the La Totorilla diatexites. In this study, a U–Pb zircon concordia age of 532.1 ± 1.7 Ma was obtained for the M2-D2 event (Fig. 10c). This is close to the crystallization age of the porphyritic facies of the El Pilón granitoid (523 ± 4 Ma, Rapela et al. 1998; 526.9 ± 4 , Stuart-Smith et al. 1999). These latter authors also dated the equigranular facies of the El Pilón granitoid, obtaining younger ages of 514 ± 3 Ma and 480 ± 4 Ma. The latter age coincides with the secondary peak of ~ 480

 Table 1. U-Pb analytical data (LA-ICP-MS) for zircons from the La Totorilla foliated porphyroblastic diatexites (sample #1017)

	CI	nemical con	tent		Radiogenic relationships						
Grain point	²³² Th (ppm)	²³⁸ U (ppm)	Th/U (mass)	²⁰⁷ Pb/ ²³⁵ U	20	²⁰⁶ Pb/ ²³⁸ U	20	rho	²⁰⁷ Pb/ ²⁰⁶ Pb	20	
C073-01*	36.6139	2011.2582	0.02	0.687	0.071	0.074	0.007	0.099	0.067	0.004	
C073-02	10.3048	821.3416	0.01	0.794	0.028	0.088	0.003	0.117	0.065	0.002	
C073-03	15.7065	2767.5682	0.01	0.652	0.033	0.077	0.003	0.105	0.062	0.002	
C073-04a	16.9772	5094.3451	0.00	0.694	0.020	0.087	0.003	0.160	0.058	0.001	
C073-04b	16.1628	2514.2200	0.01	0.836	0.025	0.103	0.004	0.155	0.059	0.001	
C073-05	23.8551	1597.6866	0.01	0.655	0.024	0.081	0.003	0.135	0.059	0.002	
C073-06	31.9736	1398.4615	0.02	0.661	0.021	0.083	0.003	0.152	0.058	0.002	
C073-08	24.3419	1710.1040	0.01	0.636	0.019	0.078	0.003	0.148	0.059	0.001	
C073-09	583.8863	1204.9394	0.48	0.779	0.026	0.091	0.003	0.129	0.062	0.002	
C073-10	48.1779	1873.8466	0.03	0.637	0.019	0.078	0.003	0.148	0.059	0.001	
C073-11	24.1560	1264.2827	0.02	0.685	0.021	0.086	0.003	0.151	0.058	0.001	
C073-12	34.0046	429.7629	0.08	0.652	0.024	0.078	0.003	0.125	0.060	0.002	
C073-13	30.1940	966.3991	0.03	0.716	0.023	0.089	0.003	0.143	0.059	0.001	
C073-14*	64.6664	517.8246	0.12	0.890	0.047	0.077	0.003	0.062	0.084	0.004	
C073-15	35.9043	1509.8859	0.02	0.715	0.023	0.085	0.003	0.134	0.061	0.002	
C073-16	61.1046	227.5518	0.27	2.242	0.083	0.198	0.008	0.094	0.082	0.003	
C073-17	12.9326	1198.6984	0.01	0.684	0.021	0.086	0.003	0.153	0.058	0.001	
C073-18	32.3410	1825.0183	0.02	0.654	0.020	0.080	0.003	0.152	0.059	0.001	
C073-20	127.4724	565.8152	0.23	1.154	0.036	0.126	0.005	0.130	0.067	0.002	
C073-21	8.7219	997.8700	0.01	0.731	0.024	0.090	0.001	0.057	0.059	0.002	
C073-22	26.4341	556.9710	0.05	0.710	0.023	0.086	0.001	0.057	0.060	0.002	
C073-23	32.1727	848.8222	0.04	0.700	0.023	0.088	0.001	0.058	0.058	0.001	
C073-24a	98.3604	530.9405	0.19	0.715	0.030	0.086	0.002	0.050	0.060	0.002	
C073-24b	102.4817	631.4298	0.16	0.790	0.029	0.094	0.002	0.056	0.061	0.002	
C073-25	147.1991	388.5811	0.38	0.963	0.032	0.109	0.002	0.049	0.064	0.002	
C073-26	181.9470	801.0550	0.23	1.817	0.058	0.181	0.003	0.052	0.073	0.002	
C073-27	45.8304	841.3768	0.05	0.748	0.028	0.093	0.002	0.058	0.058	0.002	
C073-28*	17.9246	1099.5480	0.02	0.872	0.030	0.090	0.002	0.054	0.070	0.002	
C073-29*	18.1639	1631.2444	0.01	0.686	0.023	0.075	0.001	0.064	0.066	0.002	
C073-30	173.8727	258.4629	0.67	0.912	0.038	0.104	0.002	0.053	0.063	0.002	
C073-31	22.2838	1506.3681	0.01	0.620	0.018	0.078	0.001	0.058	0.058	0.001	
C073-32	25.7554	854.5146	0.03	0.757	0.024	0.090	0.001	0.055	0.061	0.001	
C073-33	28.7862	1972.3353	0.01	0.611	0.019	0.075	0.001	0.057	0.059	0.001	
C073-34	52.0781	1466.1009	0.04	0.667	0.021	0.082	0.001	0.058	0.059	0.001	
C073-35	147.6569	540.7239	0.27	9.245	0.267	0.390	0.006	0.022	0.171	0.003	
C073-36*	94.8397	795.9518	0.12	1.010	0.047	0.092	0.002	0.032	0.080	0.003	
C073-37	17.8167	1313.3746	0.01	0.704	0.022	0.088	0.001	0.059	0.058	0.001	
C073-38	64.6409	498.6724	0.13	0.789	0.029	0.099	0.002	0.057	0.057	0.002	
C073-39	26.7936	416.9648	0.06	0.690	0.026	0.088	0.001	0.056	0.057	0.002	
C073-40	16.7423	1041.6954	0.02	0.745	0.026	0.087	0.002	0.060	0.062	0.002	
C073-41	48.2989	513.5902	0.09	0.999	0.033	0.107	0.002	0.053	0.067	0.002	
C073-42	28.6195	887.1761	0.03	0.760	0.025	0.087	0.001	0.052	0.064	0.002	
C073-43*	216.8616	605.6523	0.36	2.338	0.148	0.155	0.004	0.024	0.109	0.005	
C073-44	19.2211	1287.1331	0.01	0.660	0.024	0.076	0.002	0.064	0.063	0.002	
C073-45	48.6496	92.5804	0.53	4.834	0.170	0.312	0.005	0.031	0.112	0.003	
C073-46	10.9897	542.2814	0.02	0.764	0.027	0.090	0.001	0.054	0.061	0.002	
C073-47	17.8421	50.9659	0.35	1.794	0.089	0.171	0.004	0.042	0.076	0.004	
C073-48	55.5804	951.3273	0.06	0.818	0.025	0.098	0.001	0.057	0.061	0.001	

C073-49	63.1584	330.6425	0.19	0.718	0.027	0.085	0.002	0.057	0.061	0.002
C073-50	17.7391	857.9074	0.02	0.679	0.022	0.082	0.001	0.057	0.060	0.002
C073-51	32.7296	454.8692	0.07	0.722	0.025	0.086	0.001	0.052	0.061	0.002
C073-52	7.8867	1674.8297	0.00	0.777	0.025	0.096	0.002	0.068	0.059	0.001
C073-53	22.8315	1009.5491	0.02	0.797	0.030	0.091	0.002	0.073	0.064	0.002
C073-54	19.8520	982.0159	0.02	0.670	0.022	0.085	0.001	0.062	0.057	0.002
C073-55	38.3628	1586.1869	0.02	0.730	0.024	0.085	0.001	0.056	0.063	0.002
C073-56	16.2745	1070.9296	0.02	0.715	0.024	0.088	0.001	0.056	0.059	0.002
C073-57*	35.7085	1367.3214	0.03	0.816	0.064	0.083	0.001	0.020	0.072	0.005
C073-58*	145.4580	976.1719	0.15	0.857	0.027	0.085	0.002	0.057	0.073	0.002
C073-59	24.8178	1639.2163	0.02	0.684	0.021	0.085	0.001	0.067	0.058	0.001
C073-60	27.0527	1670.0569	0.02	0.678	0.021	0.084	0.001	0.058	0.059	0.001
C073-61*	788.3289	981.4464	0.80	1.363	0.047	0.119	0.002	0.043	0.083	0.002
C073-62	46.0246	628.7539	0.07	0.682	0.024	0.086	0.001	0.055	0.058	0.002
C073-63	18.9793	2136.1254	0.01	0.663	0.028	0.078	0.001	0.043	0.062	0.002
C073-64	18.9491	2179.3827	0.01	0.653	0.020	0.075	0.001	0.057	0.063	0.002
C073-65	18.0136	1861.8094	0.01	0.654	0.022	0.080	0.001	0.062	0.060	0.002
C073-66	33.7055	2416.6019	0.01	0.615	0.019	0.075	0.001	0.058	0.060	0.001
C073-67*	22.7157	1843.5095	0.01	0.999	0.044	0.072	0.001	0.029	0.100	0.004
C073-68	28.1710	1421.7334	0.02	0.656	0.019	0.081	0.001	0.061	0.059	0.001
C073-69	276.3475	602.1357	0.46	0.734	0.025	0.087	0.001	0.051	0.061	0.002
C073-70	29.7240	782.7374	0.04	0.736	0.027	0.089	0.001	0.054	0.060	0.002
C073-71a	17.5292	1549.9632	0.01	0.664	0.022	0.084	0.001	0.059	0.058	0.002
C073-71b	17.4525	1340.1060	0.01	0.725	0.026	0.091	0.002	0.066	0.058	0.002
C073-72	48.0917	907.1096	0.05	0.689	0.022	0.085	0.001	0.063	0.059	0.002
C073-73	100.1873	171.2029	0.59	0.692	0.030	0.087	0.002	0.057	0.058	0.002
C073-74	22.7448	1104.2682	0.02	0.785	0.027	0.098	0.002	0.072	0.058	0.001
C073-75	26.4776	2624.3081	0.01	0.681	0.021	0.085	0.001	0.066	0.058	0.001
C073-76	26.4654	142.4016	0.19	1.398	0.070	0.141	0.003	0.050	0.072	0.003
C073-77	43.3351	113.2198	0.38	0.696	0.038	0.088	0.002	0.048	0.057	0.003
C073-78	16.4330	392.2482	0.04	0.778	0.033	0.087	0.001	0.042	0.065	0.003
C073-79*	142.7202	100.8220	1.42	2.527	0.193	0.187	0.004	0.021	0.098	0.006
C073-80	25.3308	1488.8013	0.02	0.671	0.023	0.083	0.001	0.061	0.059	0.002

^{*} Analysis excluded from age calculation: > 10% discordant.

			Isotopic ag	Recommended age (Ma)				
Grain point	²⁰⁷ Pb/ ²³⁵ U	20	²⁰⁷ Pb/ ²⁰⁶ Pb	20	²⁰⁶ Pb/ ²³⁸ U	20	Preferred 2e Conc.	
C073-01*	531.07	54.63	841.98	49.59	460.95	43.71	460.95 43.71 0.87	
C073-02	593.30	20.84	787.25	22.59	543.59	20.10	543.59 20.10 0.92	
C073-03	509.85	25.56	666.25	26.58	475.47	21.31	475.47 21.31 0.93	
C073-04a	535.17	15.63	517.48	11.07	538.53	20.04	538.53 20.04 1.01	
C073-04b	617.18	18.59	563.16	13.65	631.65	24.03	631.65 24.03 1.02	
C073-05	511.26	18.45	552.19	20.12	502.24	19.69	502.24 19.69 0.98	
C073-06	515.19	16.67	525.73	14.51	512.54	20.10	512.54 20.10 0.99	
C073-08	499.80	15.08	581.79	13.02	481.74	17.66	481.74 17.66 0.96	
C073-09	585.06	19.67	674.64	17.59	560.64	20.93	560.64 20.93 0.96	
C073-10	500.57	15.17	580.33	13.03	483.04	17.76	483.04 17.76 0.96	
C073-11	529.71	16.12	525.35	11.69	530.22	19.51	530.22 19.51 1.00	
C073-12	509.42	18.85	608.54	18.30	486.69	18.73	486.69 18.73 0.96	
C073-13	548.14	17.35	550.07	12.95	547.22	20.05	547.22 20.05 1.00	
C073-14*	646.30	34.14	1290.74	64.07	477.33	18.19	477.33 18.19 0.74	

C073-15	547.49	17.82	637.18	16.58	525.73	19.26	525.73	19.26	0.96	
C073-16	1194.28	44.29	1245.26	39.86	1163.94	45.89	1163.94	45.89	0.97	
C073-17	528.95	15.90	517.62	11.39	530.94	19.43	530.94	19.43	1.00	
C073-18	510.96	15.27	563.25	13.05	499.05	18.40	499.05	18.40	0.98	
C073-20	779.31	24.51	827.05	20.68	762.16	28.66	762.16	28.66	0.98	
C073-21	557.23	18.51	561.97	15.47	554.68	8.57	554.68	8.57	1.00	
C073-22	544.80	17.64	597.09	15.61	530.98	8.07	530.98	8.07	0.97	
C073-23	538.87	17.56	509.82	12.71	544.17	8.14	544.17	8.14	1.01	
C073-24a	547.76	23.22	597.24	20.08	534.59	9.33	534.59	9.33	0.98	
C073-24b	591.20	21.71	637.13	20.73	577.70	9.95	577.70	9.95	0.98	
C073-25	684.74	22.86	739.07	20.54	666.52	9.67	666.52	9.67	0.97	
C073-26	1051.50	33.56	999.11	25.68	1073.51	17.74	1073.51	17.74	1.02	
C073-27	567.00	21.41	547.08	16.09	570.37	10.09	570.37	10.09	1.01	
C073-28*	636.78	21.69	936.12	26.72	554.14	9.86	554.14	9.86	0.87	
C073-29*	530.35	17.81	801.28	21.78	468.42	9.16	468.42	9.16	0.88	
C073-30	658.26	27.60	717.05	27.63	639.46	12.41	639.46	12.41	0.97	
C073-31	489.59	14.53	518.28	11.45	482.05	6.65	482.05	6.65	0.98	
C073-32	572.49	18.39	628.03	15.50	556.98	8.30	556.98	8.30	0.97	
C073-33	484.06	15.21	557.18	13.23	467.40	6.82	467.40	6.82	0.97	
C073-34	518.99	16.03	549.76	12.94	510.53	7.43	510.53	7.43	0.98	
C073-35	2362.58	68.26	2569.30	50.56	2124.85	31.73	2124.85	31.73	0.90	
C073-36*	708.82	33.30	1184.42	44.32	566.36	9.36	566.36	9.36	0.80	
C073-37	541.24	17.27	526.32	12.93	543.08	8.20	543.08	8.20	1.00	
C073-38	590.71	21.76	509.47	15.44	609.75	10.15	609.75	10.15	1.03	
C073-39	532.81	20.42	487.57	16.77	541.60	9.09	541.60	9.09	1.02	
C073-40	565.27	19.68	673.06	19.17	536.65	9.69	536.65	9.69	0.95	
C073-41	703.26	23.33	849.95	24.66	656.42	10.71	656.42	10.71	0.93	
C073-42	574.23	19.08	727.50	19.91	534.95	8.12	534.95	8.12	0.93	
C073-43*	1223.84	77.52	1782.91	80.61	929.82	21.29	929.82	21.29	0.76	
C073-44	514.76	18.47	691.56	24.29	474.46	9.45	474.46	9.45	0.92	
C073-45	1790.87	62.96	1836.45	55.04	1749.09	29.36	1749.09	29.36	0.98	
C073-46	576.35	20.03	647.71	20.84	557.72	8.93	557.72	8.93	0.97	
C073-47	1043.10	51.88	1094.62	51.97	1018.16	22.23	1018.16	22.23	0.98	
C073-48	607.03	18.24	631.14	14.43	600.61	8.59	600.61	8.59	0.99	
C073-49	549.46	20.68	642.12	21.03	527.48	9.58	527.48	9.58	0.96	
C073-50	525.96	17.41	610.82	16.31	507.21	7.93	507.21	7.93	0.96	
C073-51	551.88	18.94	643.51	18.67	530.60	8.04	530.60	8.04	0.96	
C073-52	584.00	18.47	567.84	14.16	588.96	10.31	588.96	10.31	1.01	
C073-53	595.39	22.54	730.47	18.30	561.85	13.61	561.85	13.61	0.94	
C073-54	520.89	17.15	494.27	13.06	528.46	8.51	528.46	8.51	1.01	
C073-55	556.44	18.58	697.20	17.55	523.86	8.48	523.86	8.48	0.94	
C073-56	547.49	18.17	566.92	15.49	544.58	8.14	544.58	8.14	0.99	
C073-57*	605.62	47.49	977.20	73.60	513.39	7.80	513.39	7.80	0.85	
C073-58*	628.61	19.69	1018.61	29.48	527.91	9.52	527.91	9.52	0.84	
C073-59	528.92	16.04	541.49	12.27	528.29	8.54	528.29	8.54	1.00	
C073-60	525.32	16.17	549.65	12.22	522.36	7.50	522.36	7.50	0.99	
C073-61*	873.27	30.37	1276.28	33.44	726.76	12.50	726.76	12.50	0.83	
C073-62	528.15	18.29	536.00	15.63	529.07	8.02	529.07	8.02	1.00	
C073-63	516.71	21.45	664.21	26.75	486.67	7.29	486.67	7.29	0.94	
C073-64	510.30	15.73	713.67	17.19	468.05	7.14	468.05	7.14	0.92	
C073-65	510.78	17.09	596.07	16.34	494.59	8.44	494.59	8.44	0.97	
20.00	0.0.70				.0 1.00	V.11	10 1.00	J. 1 1	0.01	

C073-66	486.78	14.72	589.19	13.70	467.74	6.69	467.74 6.69 0.96
C073-67*	703.20	30.64	1632.41	64.61	451.13	7.83	451.13 7.83 0.64
C073-68	512.19	15.22	574.95	12.76	500.80	7.32	500.80 7.32 0.98
C073-69	559.03	19.32	650.31	18.43	539.50	8.01	539.50 8.01 0.97
C073-70	560.13	20.77	619.20	18.43	548.73	9.18	548.73 9.18 0.98
C073-71a	517.34	17.45	520.18	13.62	519.51	8.20	519.51 8.20 1.00
C073-71b	553.81	19.57	539.34	14.91	559.20	10.40	559.20 10.40 1.01
C073-72	532.05	17.12	582.54	14.97	522.95	8.58	522.95 8.58 0.98
C073-73	533.97	23.44	515.93	21.14	540.73	10.75	540.73 10.75 1.01
C073-74	588.56	20.55	539.27	13.60	604.52	12.23	604.52 12.23 1.03
C073-75	527.40	16.07	537.51	11.58	527.81	8.53	527.81 8.53 1.00
C073-76	888.29	44.33	989.59	43.89	852.23	21.08	852.23 21.08 0.96
C073-77	536.14	29.44	506.30	25.03	545.77	11.37	545.77 11.37 1.02
C073-78	584.44	24.47	778.04	29.90	538.12	8.47	538.12 8.47 0.92
C073-79*	1279.80	97.92	1593.73	104.14	1105.75	23.79	1105.75 23.79 0.86
C073-80	521.31	17.81	572.51	14.93	511.96	8.62	511.96 8.62 0.98

Note: Conc. = concordance (1 ± 0.10) .

Ma in the KDE diagram obtained for the La Totorilla diatexites (Fig. 10b). Stuart-Smith et al. (1999) did not recognize this younger age in the porphyritic facies of the El Pilón granitoid; thus, they did not attributed it to the Famatinian magmatism common in the Sierras of La Rioja, San Luis and Córdoba. In our case, we assign this late Cambrian—early Ordovician age (~ 480 Ma) to the effects of high-temperature penetrative ductile deformation during the M3–D3 event in the La Totorilla diatexites. This last event is attributed here to the late stages of the Pampean orogeny (Guereschi and Martino 2014).

Therefore, it is interpreted that the La Totorilla anatectic body was generated in the early Cambrian under high-temperature and medium-pressure (Barrovian) conditions, at a maximum depth of 22 km, within the San Carlos Migmatitic Massif and at the northern end of the Central Granulite Belt. This occurred during the climax of the collision of the Pampia terrain with the western margin of Gondwana (Ramos et al. 2010), during the Pampean orogeny at ~ 520–530 Ma (Ramos et al. 2014 and references therein). This last orogeny could have extended to the Cambrian–Ordovician boundary, as recorded by the penetrative deformation and subsequent cooling of the La Totorilla anatectic body.

In summary, the La Totorilla foliated porphyroblastic diatexites are metamorphic rocks of an anatectic origin that recorded a complex history of metamorphism, partial melting, and deformation, representative of the tectonic evolution of the Sierras Pampeanas of Córdoba during the early Cambrian.

CONCLUSIONS

The La Totorilla body is not a porphyritic granitoid of

igneous origin, but rather consists of anatectic metamorphic rocks defined as foliated porphyroblastic diatexites. This interpretation is supported by textural evidence indicating metamorphic reactions and extensive *in situ* partial melting.

Three main stages were identified in the metamorphic evolution, following a clockwise P-T path: (a) a prograde stage (metamorphic event M1–D1), characterized by the formation of staurolite and biotite at approximately 600 °C; (b) the metamorphic peak (M2–D2), during which cordierite, potassium feldspar, and melt were generated from biotite dehydration, reaching temperatures of \sim 788 °C; and (c) finally, a retrograde stage (M3–D3) that included progressive deformation, cooling, and final hydration (M4).

The La Totorilla diatexites coexisted with the Pichanas migmatites in a high-ductility environment, transitioning toward a metamorphic complex represented by the Tuclame Banded Schists and biotite gneisses. The latter remained as xenoliths, and are interpreted as paleosome remnants and restites.

The lithological assemblage was intensely deformed by flattening under a pure shear regime, with relative mobility between bodies of contrasting lithology and rheology. As a result, the La Totorilla body was configured as a large boudin within the Pichanas migmatites, integrating the $\rm S_2$ foliation oriented N 300°, developed during deformation events D2–D3.

Based on the rheological relationships observed between xenoliths and migmatites, it is concluded that the La Totorilla diatexites were more resistant to deformation (more competent) than the xenoliths (which formed mullions at the contact), and at the same time, more rigid than the Pichanas migmatites.

The S₂ foliation, penetrative in all lithologies of the

studied area, resulted from a complex evolution involving metamorphism, anatexis, and flattening deformation. Deformation progressively waned with time and decreasing temperature, moving from intense to weaker flattening, as evidenced in tourmaline-bearing granitic veins and microstructures.

The La Totorilla body can be related to other anatectic bodies in the San Carlos Migmatitic Massif, such as El Pilón and Juan XXIII, which exhibit similar petrographic characteristics.

The flattening deformation (pure shear) found in the La Totorilla diatexites differs from the simple shear deformation found in most of the lithologies that constitute the San Carlos Migmatitic Massif.

Finally, the La Totorilla foliated porphyroblastic diatexites formed under high-temperature and medium-pressure conditions at middle-crustal levels (≤ 22 km depth), during the early Cambrian metamorphic peak (~ 532 Ma), within the northern sector of the Central Granulite Belt in the Sierras Pampeanas of Córdoba, associated with the Pampean orogeny at the southwestern margin of Gondwana.

SUPPLEMENTARY MATERIAL

Mineral chemical composition and cordierite thermometry of the La Totorilla foliated porphyroblastic diatexites (sample #1017).

ACKNOWLEDGMENTS

Financial support for this paper was provided by the following scientific institutions from Argentina: the Consejo Nacional de Investigaciones Científicas y Técnicas [CONICET, PIP 2021–11220200103191] and the Secretaría de Ciencia y Tecnología of the Universidad Nacional de Córdoba [SECyT–UNC, Consolidar PIDTA 2023–33620230100045CB]. The authors give special thanks to Maximiliano Medina for the preparation of thin sections for EPMA analysis at the LabGeo (CONICET-UNC Laboratory). The geochronological dating by Late Andes S.A. is gratefully appreciated. Constructive reviews were provided by Alfonso Sola, Paulo Marco, the associate editor Alina Tibaldi and the editor Ricardo Astini.

REFERENCES

Arnosio, M., Popridkin, C., Báez, W. and Bustos, E. 2014. El volcanismo terciario: Complejo Volcánico Pocho. In: Martino, R.D. and Guereschi, A.B. (eds.): Geología y Recursos Naturales de la Provincia de Cór-

- doba. Relatorio del 19º Congreso Geológico Argentino, 1: 623-647, Córdoba.
- Ashworth, J.R. 1975. Staurolite at anomalously high grade. Contributions to Mineralogy and Petrology 53 (4): 281–191.
- Astini, R. A. and Oviedo, N. d. V. 2014. Cubierta sedimentaria mesozoica. In: Martino, R.D. and Guereschi, A.B. (eds.): Geología y Recursos Naturales de la Provincia de Córdoba. Relatorio del 19º Congreso Geológico Argentino, 1: 435–471, Córdoba.
- Barzola, Ma.G., Tibaldi, A.M., Otamendi, J. E., Cristofolini, E.A., Schwartz, J.J., Benito, M.P., Armas P. 2021. P-T-t path reconstruction in a syn-deformational migmatization event along the north-central portion of Sierra de Comechingones, Córdoba, Argentina, Journal of South American Earth Sciences, 112 (1): 103534, https://doi.org/10.1016/j. jsames.2021.103534.
- Barbero, L. and Villaseca, C. 1992. The Layos Granite, the Hercynian Complex of Toledo (Spain): an example of parautochthonous restite-rich granite in a granulite area. Transactions of the Royal Society of Edinburgh, Earth Sciences 83: 127–138.
- Bonalumi, A., Martino, R., Sfragulla, J.A., Baldo, E., Zarco, J., Carignano, C., Tauber, A., Kraemer, P., Escayola, M., Cabanillas, A., Juri, E. and Torres, B. 1999. Hoja Geológica 3166–IV, Villa Dolores. Servicio Geológico Minero Argentino (SEGEMAR), Boletín 250: 141 p., Buenos Aires.
- Brito Neves, B.B. y Fuck, R.A. 2013. Neoproterozoic evolution of the basement of the South-American platform. Journal of South America Earth Sciences 47: 72–89.
- Brown, M. 1994. The generation, segregation, ascent and emplacement of granite magma: the migmatite-to-crustally derived granite connection in thickened orogens. Earth Science Reviews 36: 83–130.
- Brown, M. and Rushmer, T. (eds.) 2006. Evolution and differentiation of the continental crust. Cambridge University Press, 553 p., New York.
- Brown, M. 2013. Granite: from genesis to emplacement. Geological Society of America Bulletin 125 (7–8): 1079–1113, https://doi.org/10.1130/B30877.1.
- Bucher, K. and Frey, M. 1994. Petrogenesis of metamorphic rocks. 6° Edition. Complete revision of Winkler's textbook. Springer-Verlag, 441 p., Berlin, Heidelberg, New York.
- Currie, K.L. 1971. The reaction 3 cordierite = 2 garnet + 4 sillimanite + 5 quartz as a geological thermometer in the Opinicon Lake region, Ontario. Contribution to Mineralogy and Petrology 33: 215–226. https://doi.org/10.1007/BF00374064.
- Díaz Alvarado, J. 2017. Experimental early crystallization of K-feldspar in granitic systems. Implications on the origin of magmatic fabrics in granitic rocks. Geológica Acta 15 (4): 261–281.
- Gordillo, C.E. and Lencinas, A.N., 1979. Sierras Pampeanas de Córdoba y San Luis. In: Leanza, A. P. (ed.), Geología Regional Argentina, Tomo 1: 577–650. Academia Nacional de Ciencias, Córdoba.
- Gordillo, C.E. 1979. Observaciones sobre la petrología de las rocas cordieríticas de las Sierras de Córdoba. Boletín de la Academia Nacional

- de Ciencias, 53 (1-2): 2-44.
- Gordillo, C.E. 1984. Migmatitas cordieríticas de la Sierra de Córdoba; condiciones físicas de la migmatización. Miscelánea 68: 140 p. Academia Nacional de Ciencias, Córdoba.
- Goscombe, B.D, Passchier, C.W. and Hand, M. 2004. Boudinage classification: end-member boudin types and modified boudin structures. Journal of Structural Geology 26: 739-763.
- Guereschi, A.B. and Martino, R.D. 2014. Las migmatitas de las Sierras de Córdoba. In: Martino, R.D. y Guereschi, A.B. (eds.), Geología y Recursos Naturales de la Provincia de Córdoba, Relatorio del 19º Congreso Geológico Argentino, 1: 67-94. Asociación Geológica Argentina, Córdoba.
- Guereschi, A. B., Palavecino. A. and Martino, R. D. 2024. Petrología, deformación de alta temperatura y edad de las diatexitas cordieríticas La Totorilla, Macizo San Carlos, Sierras Pampeanas de Córdoba. 6° Simposio de Tectónica Preandina, 22° Congreso Geológico Argentino, Libro de Resúmenes: 1255-1256, San Luis.
- Guidotti, C.V., 1984. Micas in metamorphic rocks. In: Baileys, S.W. (ed.), Reviews in Mineralogy, Mineralogical Society of America 13: 357-468, Washington.
- Holness, M.B. 2008. Decoding migmatite microstructures. In: Sawyer, E.W and Brown, M. (eds.), Working with migmatites. Short Course Series 38: 57-76. Quebec.
- Holness, M.B., Cesare, B. and Sawyer, E.W. 2011. Melted rocks under the microscope: microstructures and their interpretation. Elements 7: 247-252. https://doi.org/10.2113/gselements.7.4.247.
- Hoskin, P. W. and Schaltegger, U. 2003. The composition of zircon and igneous and metamorphic petrogenesis. Reviews in Mineralogy and Geochemistry 53 (1): 27-62. https://doi.org/10.2113/0530027.
- Lagorio, S.L., Vizán, H. and Geuna, S. 2014. El volcanismo alcalino cretácico. In Martino, R.D. and Guereschi, A.B. (eds.): Geología y Recursos Naturales de la Provincia de Córdoba. Relatorio del 19º Congreso Geológico Argentino, 1: 473-511, Córdoba.
- Lescano, V.A. 2019. Petrología y estructura de la Migmatita Rumi Huasi, Macizo de San Carlos, Sierras Pampeanas de Córdoba. Trabajo Final, Hemeroteca del Departamento de Geología, Facultad de Ciencias Exactas, Físicas y Naturales, Universidad Nacional de Córdoba (unpublished), 57 p., Córdoba.
- Lira, R. and Sfragulla, J. 2014. El magmatismo devónico-carbonífero: El batolito de Achala y los plutones menores al norte del cerro Champaquí. In Martino, R.D. y Guereschi, A.B. (eds.), Geología y Recursos Naturales de la Provincia de Córdoba. 19º Congreso Geológico Argentino, Relatorio 1: 293–347, Córdoba.
- Ludwing K.R. 2003. User's Manual Isoplot 3.00. A Geochronological Toolkit for Microsoft Excel. Geochronology Center Special Publication 4, Berkeley.
- Martino, R.D. 2003. Las fajas de deformación dúctil de las Sierras Pampeanas de Córdoba: una reseña general. Revista de la Asociación Geológica Argentina 58 (4): 549–571.

- Martino, R.D. 2009. Mulliones en venas y plutones graníticos menores: posibles causas de su génesis. 14° Reunión de Tectónica, Resúmenes, p. 24, Río Cuarto.
- Martino, R. D. and Guereschi, A. B. 2014. La estructura neoproterozoica-paleozoica inferior del complejo metamórfico de las Sierras de Córdoba. In: Martino, R.D. and Guereschi, A.B. (eds.), Geología y Recursos Naturales de la Provincia de Córdoba, Relatorio del 19º Congreso Geológico Argentino, 1: 95–128. Asociación Geológica Argentina, Córdoba.
- Martino, R.D., Guereschi, A.B. and Sfragulla, J. 1997. Las anatexitas y las vetas auríferas de Río Hondo, sector sudoriental del Macizo de San Carlos, Córdoba, Argentina. Revista de la Asociación Geológica Argentina 52 (4): 433–450.
- Martino, R.D., Guereschi, A.B. and Horwitz, P.G. 2004. Estructura interna y yacencia del plutón anatéctico "Juan XXIII", Macizo de San Carlos, Sierras de Córdoba. 12° Reunión sobre Microtectónica y Geología Estructural, Resúmenes: p. 23, Cafayate.
- Martino, R.D., Guereschi, A.B. and Mogessie, A. 2005. Condiciones retrógradas del cuerpo de diatexitas Juan XXIII, Macizo de San Carlos, Sierra Grande, Córdoba. 16° Congreso Geológico Argentino, Actas 1: 881–886, La Plata.
- Martino, R. D., Guereschi, A. B. and Sfragulla, J. A. 2009. Petrology, structure and tectonic significance of the Tuclame banded schists in the Sierras Pampeanas of Córdoba and its relationship with the metamorphic basement northwestern Argentina. Journal of South American Earth Sciences, 27: 280–298.
- Mehnert, K.R. 1968. Migmatites and the origin of granitic rocks. Elsevier, 393 p., Amsterdam, London, New York.
- Miller, C.F., Stoddard, E.F., Bradfish, L.J. and Dollase, W.A. 1981. Composition of plutonic muscovite: genetic implications. Canadian Mineralogist 19: 25–34.
- Nachit H., Ibhi A., Abia E.H. and Ben Ohod M. 2005. Discrimination between primary magmatic biotites, reequilibrated biotites and neoformed biotites. Comptes Rendu Geosciences 337: 1415–1420.
- Nicollet, C. 2010. Métamorphisme et Géodynámique. Cours et exercices corrigés. Dunod Editions, 288 p., Paris.
- Otamendi, J.E., Castellarini, P.A., Fagiano, M.R., Demichelis, A.H. and Tibaldi, A.M. 2004. Cambrian to Devonian geologic evolution of the Sierra de Comechingones, eastern Sierras Pampeanas, Argentina: evidence for the development and exhumation of continental crust on the proto-Pacific margin of Gondwana. Gondwana Research 7: 1143–1155.
- Palavecino, A. 2020. Petrología y estructura del cuerpo anatéctico La Totorilla, Macizo de San Carlos, Sierras de Córdoba. Trabajo Final, Hemeroteca del Departamento de Geología, Facultad de Ciencias Exactas, Físicas y Naturales, Universidad Nacional de Córdoba, 74 p. (unpublished), Córdoba.
- Pankhurst, R. J. and Rapela, C. W. (eds.), 1998. The proto-Andean margin of Gondwana. Geological Society of London, Special Publications

- 142, 383 p. Doi: 10.1144/GSL.SP.1998.142.01.01.
- Passchier, C.W., and Trouw, R.A. 2006. Microtectonics. 2nd, Revised and Enlarged Edition. Springer–Verlag, 344 p., Berlin, Heidelberg.
- Pawley, M., Reid, A., Dutch, R. and Preiss, W. 2015. Demystifying migmatites: an introduction for the field-based geologist. Applied Earth Science 124 (3): 147–174. https://doi.org/10.1179/174327581 5Y.0000000014.
- Perarnau, M., Gilbert, H., Alvarado, P., Martino, R. y Anderson, M. 2012. Crustal structure of the Eastern Sierras Pampeanas of Argentina using high frequency local receiver functions. Tectonophysics 580: 208-217. http://dx.doi.org/10.1016/j.tecto.2012.09.021.
- Pereira, M. D. and Bea, F., 1994. Cordierite-producing reactions in the Peña Negra complex, Avila Batholith, Central Spain: The key role of cordierite in low-pressure anatexis. Canadian Mineralogist 32: 763–780.
- Ramos, V.A., Vujovich, G., Martino, R. and Otamendi, J. 2010. Pampia: a large cratonic block missing in the Rodinia supercontinent. Journal of Geodynamics 50: 243–255. https://doi.org/10.106/j.org.2010.01.019.
- Ramos, V.A., Martino, R.D., Otamendi, J.E. and Escayola, M.P. 2014. Evolución Geotectónica de las Sierras Pampeanas Orientales. In: Martino, R.D. and Guereschi, A.B. (eds.), Geología y Recursos Naturales de la Provincia de Córdoba, Relatorio del 19º Congreso Geológico Argentino, 2: 965–976. Asociación Geológica Argentina, Córdoba.
- Rapela, C. W., Pankhurst, R. J., Casquet, C., Baldo, E., Saavedra, J., and Galindo, E., 1998. The Pampean orogeny of the southern proto-Andes: Evidence for Cambrian continental collision in the Sierras de Córdoba. In: Pankhurst, R. J., and Rapela, C. W. (eds.), The Proto-Andean margin of South America. Geological Society of London, Special Publications 142: 181–217.
- Rapela, C.W., Baldo, E.G., Pankhurst, R.J. and Saavedra, J. 2002. Cordieritite and leucogranite formation during emplacement of highly peraluminous magma: the El Pilón Granite Complex (Sierras Pampeanas, Argentina). Journal of Petrology 43: 1003–1028.
- Rubatto, D. 2002. Zircon trace element geochemistry: partitioning with garnet and the link between U–Pb ages and metamorphism. Chemical Geology 184: 123–138.
- Sawyer, E. W. 1994. Melt segregation in the continental crust. Geology 22: 1019–1022.
- Sawyer, E.W. 2001. Melt segregation in the continental crust: distribution and movement of melt in anatectic rocks. Journal of Metamorphic Geology 19: 291–309.
- Sawyer, E.W. 2008a. Atlas of migmatites. NRC Research Press, Special Publication 9: 386 p., Ottawa–Ontario.
- Sawyer, E.W. (ed.). 2008b. Working with migmatites. Mineralogical Association of Canada, Short Course Series, 38: 158 p., Quebec.
- Siegesmund, S., Steeken, A., Martino, R.D., Wemmer, K., López de Luchi, M., Frei, R., Prensnyako, S. and Guereschi, A.B. 2010. Times constraints on the tectonic evolution of the Eastern Sierras Pampeanas (Central Argentina). International Journal of Earth Sciences

- (Geologische Rundschau) 99: 1199-1226.
- Silva, D., Piazolo, S. and Daczko N.R. 2023. Trapped K-feldspar phenocrysts as a signature of melt migration pathways within active high-strain zones. Journal Metamorphic Geology 41 (3): 351–375. https://doi.org/10.1111/jmg.12698.
- Sims, J.P., Ireland, T.R., Camacho, A., Lyons, E., Pieters, P.E., Skirrow, R.G., Stuart-Smith, P.G., y Miró, R. 1998. U–Pb, Th–Pb and Ar–Ar geochronology from the southern Sierras Pampeanas, Argentina: implications for the Palaeozoic tectonic evolution of the western Gondwana margin. In: Pankhurst, R.J., Rapela, C.W. (eds.), The Proto-Andean Margin of Gondwana. Geological Society of London, Special Publications 142: 259–281.
- Sláma, J., Košler, J., Condon, D. J., Crowley, J. L., Gerdes, A., Hanchar, J. M., Horstwood, M. S. A., Morris, G. A., Nasdala, L., Norberg, N., Schaltegger, U., Schoene, B., Tubrett, M. N. and Whitehouse, M. J. 2008. Plešovice zircon A new natural reference material for U–Pb and Hf isotopic microanalysis. Chemical Geology 249: 1–35. Doi: 10.1016/j.chemgeo.2007.11.005.
- Sokoutis, D. 1990. Experimental mullions at single and double interfaces. Journal of Structural Geology 12 (3): 365–373.
- Spear, F.S., Kohn, M.J. and Cheney, J.T. 1999. P–T paths from anatectic pelites. Contributions to Mineralogy and Petrology 134 (1): 17-32.
- Speer, J.A., 1984. Micas in igneous rocks. In: Bailey, S.W. (eds.), Micas. Reviews in Mineralogical Society of America, 13: 299-356, Washington
- Stacey J.S. and Kramers J.D. 1975. Approximation of terrestrial lead isotope evolution by a 2-stage model. Earth and Planetary Science Letters 26 (2): 207–221.
- Stuart-Smith, P.G., Camacho, A., Sims, J.P., Skirrow, R.G., Lyons, P., Pieters, P.E., Black, L.P. Miró, R. 1999. Uranium–lead dating of felsic magmatic cycles in the southern Sierras Pampeanas, Argentina: Implications for the tectonic development of the proto-Andean Gondwana margin. In Ramos, V.A. and Keppie, J.D. (eds.), Laurentia–Gondwana Conections before Pangea. Geological Society of America, Special Papers 336: 87–114, Boulder, Colorado.
- Sureda, R.J. 1978. Las vetas de plomo, plata y zinc del Distrito Minero "El Guaico" en la provincia de Córdoba, República Argentina. Revista de la Asociación Geológica Argentina 33 (4): 299–344.
- Trooper, P., Wyhlidal, S., Haefeker, U.A. and Mirwald, P.W. 2017. An experimental investigation of Na incorporation in cordierite in low P/high T metapelites. Mineralogy and Petrology 112: 199–217. DOI 10.1007/s00710-017-0522-2.
- Villaseca, C., Pérez Soba, C., Merino, E., Orejana, D., López García, J.A and Billstrom, K. 2008. Contrasted crustal sources for peraluminous granites of the segmented Montes de Toledo Batholith (Iberian Variscan Belt). Journal of Geosciences 56: 263–280.
- Vermeesch, P. 2018. Isoplot R: a free and open toolbox for geochronology. Geoscience Frontiers 9: 1479–1793. https://doi.org/10.1016/j.gsf.2018.04.001.

- Vernon R.H. 2011. Microstructures of melt-bearing metamorphic rocks. In: Van Reenen, D.D., Kramers, J.D., McCourt, S. and Perchuk, L.L. (eds.), Origin and Evolution of Precambrian High-Grade Gneiss Terrains, with Special Emphasis on the Limpopo Complex of Southern Africa. Geological Society of America Memoir 207: 1–12. https://doi.org/10.1130/2011.1207(01).
- Vanderhaegue, O. 2001. Melt segregation, pervasive melt migration and magma mobility in the continental crust: the structural record from pores to orogens. Physics and Chemistry of the Earth (A), 26 (4–5): 213–223.
- Whitney, D. and Evans, B. 2010. Abbreviations for names of rock-forming minerals. American Mineralogist 95: 185–187.
- Wiedenbeck, M., Hanchar, J. M., Peck, W. H., Sylvester, P., Valley, J., Whitehouse, M., Kronz, A., Morishita, Y., Nasdala, L., Fiebig, J., Franchi, I., Girard, J.-P., Greenwood, R.C., Hinton, R., Kita, N., Mason, P.R.D., Norman, M., Ogasawara, M., Piccoli, P.M., Rhede, D., Satoh, H., Schulz-Dobrick, B., Skår, O., Spicuzza, MJ., Terada, K., Tindle, A., Togashi, S., Vennemann, T., Xie, Q. and Zheng, Y.-F. 2004. Further caracterisation of the 91500 zircon crystal. Geostandards and Geoanalytical Research 28 (1): 9–39. https://doi.org/10.1111/j.1751-908X.2004.tb01041.x.
- Yardley, B. y Warren, C. 2021. An Introduction to Metamorphic Petrology. Cambridge University Press, 333 p., Cambridge.